Safety Study Related to Hydrogen Leakage from Fuel Cell Systems

Jiaqing He

A Thesis

in

The Department

of

Mechanical and Industrial Engineering

Presented in Partial Fulfillment of the Requirements
For the Degree of Master of Applied Science (Mechanical Engineering) at
Concordia University
Montreal, Quebec, Canada

January 2017

CONCORDIA UNIVERSITY

School of Graduate Studies

This is to certify that this thesis is prepared

By: Jiaqing He

Entitled: Safety Study Related to Hydrogen Leakage from Fuel Cell Systems

and submitted in partial fulfillment of the requirements for the degree of

Master of Applied Science (Mechanical Engineering)

complies with the regulations of the University and meets the accepted standards with respect to originality and quality.

Signed by the final examining committee:

Dr. Charles Basenga Kiyanda   Chair

Dr. Hua Ge   Examiner

Dr. Lyes Kadem   Examiner

Dr. Hoi Dick Ng   Supervisor

Dr. Liangzhu Wang   Supervisor

Approved by   _____

Chair of Department or Graduate Program Director

_____

Dean of Faculty

Date   _____

ABSTRACT

Safety study related to hydrogen leakage from fuel cell systems

Jiaqing He

The main challenge for the wide spread use of hydrogen in fuel cell systems is the safety concerns due to its ease of leaking, low-energy ignition, large flammability range, high buoyancy and diffusion rate in air. To alleviate concern of explosion during experiments, scientists are using helium as a stimulant for hydrogen safety studies. However, the equivalent behavior between the two gases only relies on numerical or experimental results, and the similarity is not connected by a theoretical correlation. This thesis assesses similarity relations using helium for hydrogen studies and develops a theoretical helium plume model. Meanwhile, a case study of leakage in fuel cell vehicles is simulated by Computational Fluid Dynamics (CFD).

The accuracy of three different correlations, i.e., equal volumetric flow rate, equal buoyancy and equal concentration between helium and hydrogen was compared by CFD simulations validated by helium experiment in a 1/4 sub-scale residential garage model. The accuracy of these different methods at different leakage rate, stage of release, ventilation method and location was discussed. An updated theoretical helium plume model was validated by PIV (Particle Image Velocimetry) experiment and CFD. It is found that the new model could be used in estimating the plume size and velocity. In the case study of hydrogen leakage inside a FCV (Fuel Cell Vehicle), ventilation and sunroof show critical effect to reduce the level of hydrogen concentration accumulation.

ACKNOWLEDGEMENT

Table of Contents

List of Figures

List of Tables

NOMENCLATURE

b	Plume radius [m]
B	Buoyancy flux [m^4/s^3]
C	Volumetric concentration
g	Gravity [m/s^2]
$\dot{m}$	Mass flow rate [kg/s]
n	correlation exponent
Q	Volumetric flow rates [m^3/s]
u	Plume velocity [m/s]
v	Air entrainment velocity [m/s]
z	Height [m]

Greek letters

α	Entrainment ratio
ρ	Density [kg/m^3]

Acronyms

ACH   Air changes per hour

PEMFC   Proton Exchange Membrane Fuel Cell

CFD   Computational Fluid Dynamics

LES   Large Eddy Simulation

PIV   Particle Image Velocimetry

1 Introduction

1.1 Background

Hydrogen is considered one of the leading fuels as a renewable and environment friendly energy carrier within the next years [1]. Fuel cells using hydrogen present significant advantage in reducing the amount of carbon dioxide generated by transportation systems and higher efficiency when compared with the traditional fossil fuels.

The first fuel cell was developed by William Grove in 150 years ago. He brought forward the idea to investigate the reverse version of electrolysis. The first successful implementation was carried by Francis Bacon in 1932. NASA applied the fuel cell in spacecraft as electric generators, which counts as the first commercial use of fuel cells. Today, fuel cells are used for primary and backup power in commercial, industrial, transportation and residential buildings.

1.2 Hydrogen applications

Hydrogen was primarily used in petroleum refining, ammonia production and metal refining [2]. In the future, hydrogen is likely to be used as an energy source in all applications where fossil fuels are used today. Substantial on-going research around the world explores the use of fuel cells into three broad areas: portable power generation, stationary power generation, and power for transportation. The main future use of hydrogen is dominantly in transportation.

A fuel cell vehicle (FCV) or fuel cell electric vehicle (FCEV) is a type of automobile that uses a fuel cell to power electric motor. FCV mostly uses oxygen from air and compressed hydrogen emitting only water and heat, but no tailpipe pollutants. In 1966, General Motors developed the

Chevrolet Elctrovan, first fuel cell road vehicle, which had a range of 120 miles with a fuel cell [3]. The automobile manufactures were interested in the application of fuel cell by the 1990s.

FCVs look like conventional vehicles from outside, but inside they contain technologically advanced components. The most obvious difference is the fuel cell stack that converts hydrogen gas stored with oxygen from the air into electricity to drive the electric motor that propels the vehicle. The major components of a typical FCV are illustrated below.

Power Control Unit
Governs the flow of electricity

Fuel Cell stack
Converts hydrogen gas and oxygen into electricity to power the electric

Hydrogen Storage Tank
Stores hydrogen gas compressed at extremely high pressure to increase driving range

Electric Motor
Propels the vehicle more quietly, smoothly, and efficiently than an internal combustion engine and requires less maintenance

Figure 1.1 Main components of a typical FCV

[Source : https://www.fueleconomy.gov/feg/fuelcell.shtml]

USA is one of the leading countries for the stationary application of hydrogen energy. In 2003, President Bush announced that the USA would support research and development into hydrogen

energy and FCV (fuel cell vehicle) would be the replacement for internal combustion engine vehicles using gasoline. He believed that this technology would reduce air pollution as the only by-product from hydrogen fuel cell is water.

Governor of California signed Executive Order B-16-2012, which supports and accelerates the commercialization of fuel cell vehicle. This plan contains three main stages: First, society will be ready for FCV in 2015. Second, there will be sufficient infrastructure to support one million FCV in 2020. Third, the market will expand in 2025 and more than 1.5 million FCV will be derived on the road. These stages provide the solution of how these complications can be bridged [4].

Typical elements of a hydrogen fueling station is shown in Fig. 1.2. Hydrogen is often produced from petrochemical and delivered to the hydrogen station with pipeline, ship or road tanker. A control system in the station is then used to manage transfer and storage of hydrogen. The liquid hydrogen from the pipeline or tanker is received by the receiving port. Heat exchanger changes the liquid hydrogen to gas and compressor compresses it to 350 or 750 bar for storage at high pressure. Dispensers fill the on-board hydrogen tanks of fuel cell vehicles through a 350 or 750 bar nozzle. The process of refueling vehicles with hydrogen is similar to filling a compressed natural gas (CNG) vehicle.
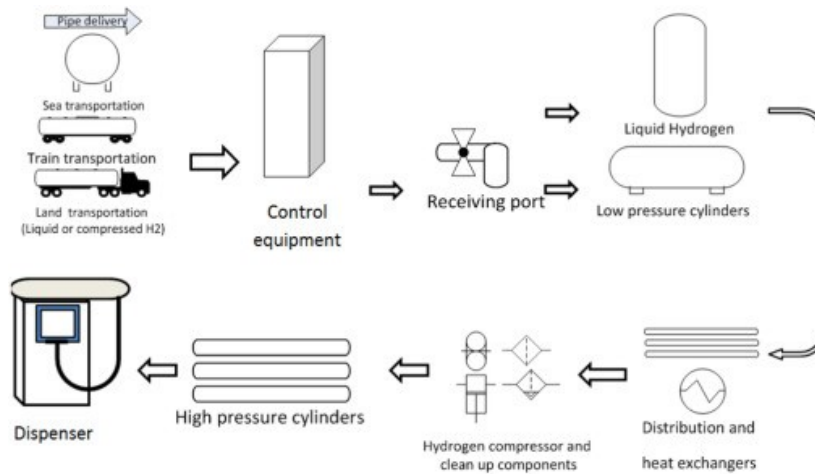
Figure 1.2 Typical elements of a hydrogen fuelling station with hydrogen delivery [5]

It can be seen from Table 1.1 that North America has the largest number of fueling station numbers around the world. 81 of them are located in USA, 13 stations located in Canada and just one in Mexico. Europe is second in term of the number of hydrogen stations, with 77 stations spread across 17 countries, followed by Asia with 51 stations in nine countries. There are only two stations in South America and no service in Australia [4, 8].

Table 1.1 Hydrogen fuelling station numbers around the world [5-11]

	North America	Europe	Asia	Australia	South America
Station numbers	94	77	51	0	2

Figure 1.3 Hydrogen fuelling station around the world

Japan spent a total of $4.1 billion in 14-years period from 2002 to 2015 [10]. The USA spent a total of $1.8 billion during the same period and Europe pledges a similar amount. The budget of Japan is twice as much. The government of Japan realized it was necessary to speed up R&D program in order to reduce fuel cell cost, improve efficiency and increase durability. Currently, fuel cell policy in Japan was supported by a cluster of ministries, including the Ministry of Education, Culture, Sports, Science and Technology (MEXT), and in other cases were directed by various Prime Ministers and the Prime Minister's Council for Science and Technology Policy [10].

The American Society of Mechanical Engineer (ASME) and U.S. Department of Energy set standards for hydrogen stationary application and transport [2]. ASHARE 62.2 puts the ventilation standard of FCV in the same category of CNG vehicles [13]. However, there is no specific standard of ventilation for hydrogen fuel vehicles.

The above section reviewed the state of application of hydrogen energy. The numbers of FCV is estimated to keep increasing in the near future. The network of hydrogen fueling station will expand when FCV gains market acceptance and grows. Many countries spent huge budget on the

R&D of hydrogen technology, creating a global hydrogen fuel cell race in the process. But there is no specific standard related to ventilation of hydrogen fuel vehicles.

1.3   Safety issues of hydrogen leakage

Fuel cells using hydrogen present significant advantage in reducing the amount of carbon dioxide emissions generated by transportation systems and have higher efficiency when compared with traditional fossil fuels [14]. However, the storage and use of hydrogen pose unique challenges due to its ease of leaking, low-energy ignition, a wide range of combustible fuel-air mixtures, high buoyancy and diffusion rate in air [15]. But hydrogen is not more or less dangerous than other flammable fuels such as gasoline and natural gas; it is imperative that all flammable fuels should be carefully utilized. Table 1.2 shows the comparison of hydrogen to other flammable fuels.

Table 1.2 Fuel flammability comparisons [16]

	Hydrogen	Gasoline Vapor	Natural Gas
Flammability Limits (in air)	4-74%	1.4-7.6%	5.3-15%
Explosion Limits (in air)	18.3-59 %	1.1-3.3%	5.7-14%
Ignition Energy (mJ)	0.02	0.2	0.29
Flame Temperature in air (°C)	2045	2197	1875
Stoichiometric Mixture (most easily ignited in air)	29%	2%	9%

Hydrogen is colorless and odorless and is about 14 times lighter than air, and diffuses faster than any other gas. While cooling, hydrogen condenses to liquid at -253 °C and to solid at -259 °C. Ordinary hydrogen is the lightest substance known with buoyancy in air of 1.2 kg/m³ density. Moreover, the gaseous hydrogen has one of the highest heat capacity (14.4 kJ/kg K).

A full deployment of hydrogen as the preferred energy carrier will largely be influenced by the public acceptance of hydrogen mainly based on safety concerns for both storage, transmission and application (as vehicle fuel or in-home use). The main hazard is in its leaking, causing a fire or explosion, which is the major issues affecting the acceptance of hydrogen for public use.

1.4   Hydrogen and helium similarity study

Due to the close properties between helium and hydrogen, some researchers use helium to conduct experiments in some safety study of hydrogen [17]. Table 1.3 presents the properties of hydrogen and helium.

Table 1.3 Properties of hydrogen and helium

Property	Hydrogen	Helium
Molecular weight	2.01594	4.00260
Density of gas at 0 °C and 1 atm	0.08987 kg/m^3	0.1678 kg/m³
Melting temperature	−259 °C	-272 °C
Boiling temperature at 1 atm	−253 °C	-269 °C
Thermal conductivity at 25 °C	0.019 kJ/kg	0.014 kJ/kg
Viscosity at 25 °C	0.000892 cP	0.00019 cP
Heat capacity (C_p) of gas at 25 °C	14.3 kJ/(kg °C)	5.19 kJ/(kg °C)

Safety analysis against leakages of hydrogen in different scenarios using Computational Fluid Dynamics (CFD) tools have been developed in recent years such as fueling station [18], hydrogen laboratory [19] and tunnels [20].

Prasad et al. [17] from the Fire Research Division, National Institute of Standards and Technology (NIST) evaluated the ability of FDS (Fire Dynamics Simulator), which simulates a number of cases on predicting the release and dispersion behavior of hydrogen, when accidentally released in a partially confined space. In order to conduct the experiments safely, helium was chosen as a surrogate. In a sub-scaled residential garage enclosure, helium gas was released from two different heights, with two different opening locations, different flow rates and release times. Seven sensors on the same horizontal location with different heights measured helium concentrations. In this study, a 1/4 scale experimental chamber with interior dimensions of $1.5 \times 1.5 \times 0.745$ m based on the dimensions of two-car residential garage $6.1 \times 6.1 \times 3.05$ m was constructed, from 1.25 cm thick plexiglas (Fig. 1.4).
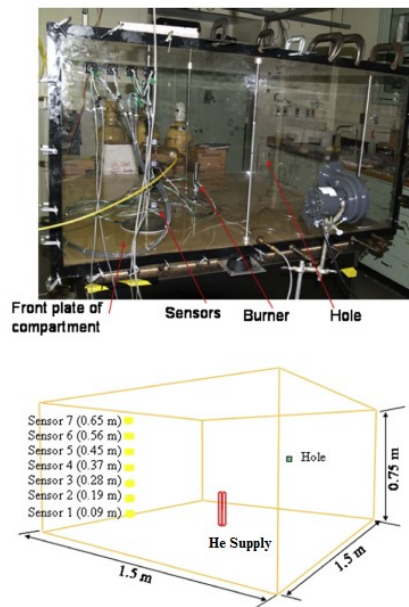
Figure 1.4 Experiment setup [17]

The height of helium injector was 207 mm, above the center of the floor with a diameter of 36 mm and a cross-sectional area of 10.2 cm². Helium flow was controlled by a mass flow controller.

Helium flow rates were calculated and scaled to the leakage rate of a typical 5 kg of hydrogen from a fuel tank in 1 hour and 4 hours, which were respectively 14.95 L/min and 3.74 L/min [17].

The paper of Prasad et al. describes a typical residential garage which considering the garage door and windows. As a result, they suggested that for a sub-scale chamber, outlet sizes were chosen to have areas that can satisfy minimum ventilation requirements for residential garages, which was 3 air changes per hour (ACH) with pressure differential of 4 Pa. An outlet with size of 2.34×2.32 cm (cross-sectional area of 5.43 cm²) and another outlet with size of 1.56×2.32 cm (cross-sectional area 3.62 cm²) were used to compare experimental data and simulation predictions.

Prasad et al. [17] simulates this study with NIST Fire Dynamic Simulator (FDS) which was developed for computing fire driven flows. The buoyant plume flowed directly to the ceiling with a horizontal spread behavior both in experiment and simulation results. Because helium was released into the chamber, air inside the chamber was pushed outwards through the holes as helium concentration increased towards the ceiling.

Sensitivity study was conducted to understand the effect of each configuration on the concentration of helium. Results showed that increasing the mass flux of helium by 10%, increased the predicted concentration of helium by 7.4%, for both sensors which were located 9.3 cm (Sensor 1) and 65 cm above the floor (Sensor 7). Reducing the injector diameter by 25%, the predicted helium concentration increased by 2.5% for both sensors 1 and 7 [17].

The effect of changing the hole size and the location of the holes on the helium concentration was also shown in this study. Reducing the hole size by 25% only made minor differences during the release which is less than 2.5%. On the contrary, the location of the leaks has a large effect on the concentration. Comparing the helium volume fraction between the cases having one single leak in

9

the center of ceiling and the case with two holes in the front wall (one at the top and one at the bottom), the concentration of sensor 1 has a 49.5% difference and sensor 7 has a 25.2% difference. Results indicate that the location of the leaks has a large effect on the helium concentration inside the compartment, while the size of the hole has a smaller effect on the results [17].

The authors also conducted a resolution study to verify the effect of mesh grids in vertical and horizontal directions. Changing the grid size from 1.55 cm to 1.16 cm, the relative difference during the release was approximately 7.5%. The helium concentration increases as the grid density increases and better matches the experiment data [17].

Swain et al. [21] proposed the hydrogen risk assessment method (HRAM) to simulate hydrogen leakage with CFD model validated by helium experiment data. This method was developed to determine the potential health and safety implications of a hydrogen leak [21]. The HRAM can be used for the ventilation design of buildings which have hydrogen-fueled equipments. This method can also be used to determine optimal hydrogen sensor locations for safety study.

Light gas leakages can be categorized by the space surrounding the leak. The classifications for the space surrounding the leaks are identified as enclosed, partially enclosed, and unconfined spaces. The risk of explosion is mainly affected by the total volume of hydrogen leaking for enclosed surrounding rather than the volume flow rate of hydrogen.

The leaking hydrogen is expected to rise towards the ceiling and then diffuses back towards the lower section. If the total volume of hydrogen leakage is less than 4.1% of the volume of the enclosure, the resulting risk of combustion would be expected to decrease to zero as the hydrogen becomes homogeneously dispersed into the enclosure. On the other hand, if the total volume of hydrogen leakage is higher than 4% but less than 75% of the volume of the enclosure, the risk of

combustion would be expected to continue until the enclosure is vented otherwise combustion could occur [21].

Swain et al. [21] have several general findings. For simple enclosures, single or double vented, the concentration of hydrogen and helium are the same for areas near the ceiling but not in close to the original leak or a vent. This phenomenon is more obvious when it is in steady condition. Besides, for area near a vent or leak origin, the concentration of hydrogen or helium may fluctuate in a large range due to instabilities in flow, which is more noticeable in the flow up a chimney [21].

Previous study has shown that using helium gas to validate CFD models could also be used to predict the dispersion behavior and concentration of hydrogen gas in a leakage scenario [21]. Both helium and hydrogen will behave similarly when released into partial enclosures. Therefore, the design of structures containing potential hydrogen gas leaks, can be evaluated using a CFD model which has been validated using helium leakage and concentration data. The HRAM method is explained as follows [21]:

1. Simulation of the leakage scenario with helium, measuring helium concentration versus time at various locations while supplying helium at the expected hydrogen rate.

2. Verification of a CFD model of the leakage scenario using the helium experimental data.

3. Prediction of the dispersion behavior and the concentration of hydrogen using the CFD model.

4. Determination of risk from the spatial and temporal distribution of hydrogen [21].

Choi et al. [22] used CFD tools to analyze the dispersion process of hydrogen leaking from an FCV in an underground parking garage and to assess the hazards and risks of a leakage accident.

The hydrogen concentration and flammable region were predicted. The authors also performed a parametric study which changed the flow rate of hydrogen to study the dispersion based on temporal evolution of the flammable region and the effect of ventilation fans.
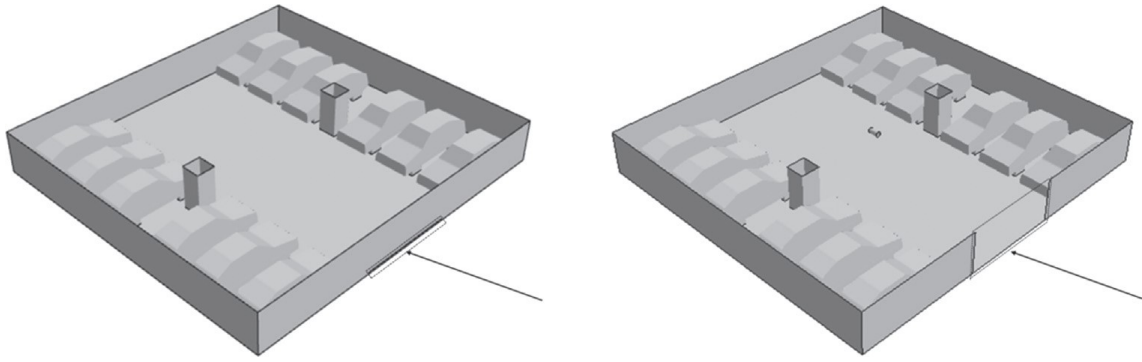
Figure 1.5 Domain and boundary condition considering a closed entrance (left) and open entrance (right) [22]

As indicated in Fig. 1.5, two different configurations were considered with different shape of the entrance and the existence of an indoor ventilation fan. The size and discharge rate of the ventilation fan is based on the specification of common commercial fans. The leakage rates of hydrogen are the volume flow rate of hydrogen with energy equivalent to a gasoline leakage regulated by U.S. FVSS 301, which has been used in several previous studies and is equivalent to volume flow rate $Q = 131$ L/min [22].

A commercial CFD software STAR-CCM + V5.06 was used in the study of Choi et al. [22]. Polyhedral elements are chosen for the computational grids. The total mesh elements is around 2 million for the case with the fan and 3 million for the case without a fan. A Linux cluster with Intel Xeon Quad-Core 2.4 GHz 64-bit processor was used to perform the simulations [22].

Figure 1.6 presents the time history of the volumetric ratio in the flammable region for different leakage flow rates. The time when the rapid change begins is delayed as the leakage rate decreases. This is related to the fast diffusion velocity of hydrogen and accumulation near the ceiling. The hydrogen concentration is increasing uniformly near the ceiling, as the hydrogen is accumulated. When the volume fraction of hydrogen is close to 4% (the lower flammable limit), the volume of the flammable region rapidly increases [22].

(a)

(b)
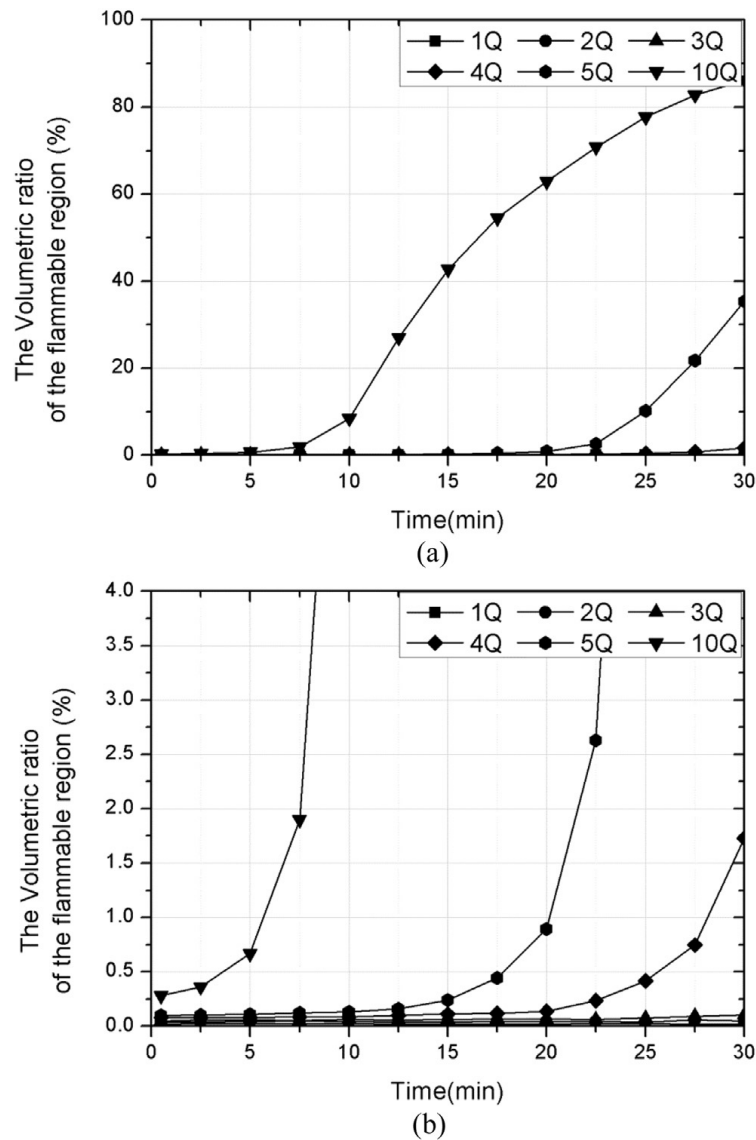
Figure 1.6 Time history of the volumetric ratio of the flammable region for different leakage flow rate [22]

(a) Without fan   (b) 20 m³/min   (c) 40 m³/min   (d) 60 m³/min

(e) Without fan   (f) 20 m³/min   (g) 40 m³/min   (h) 60 m³/min
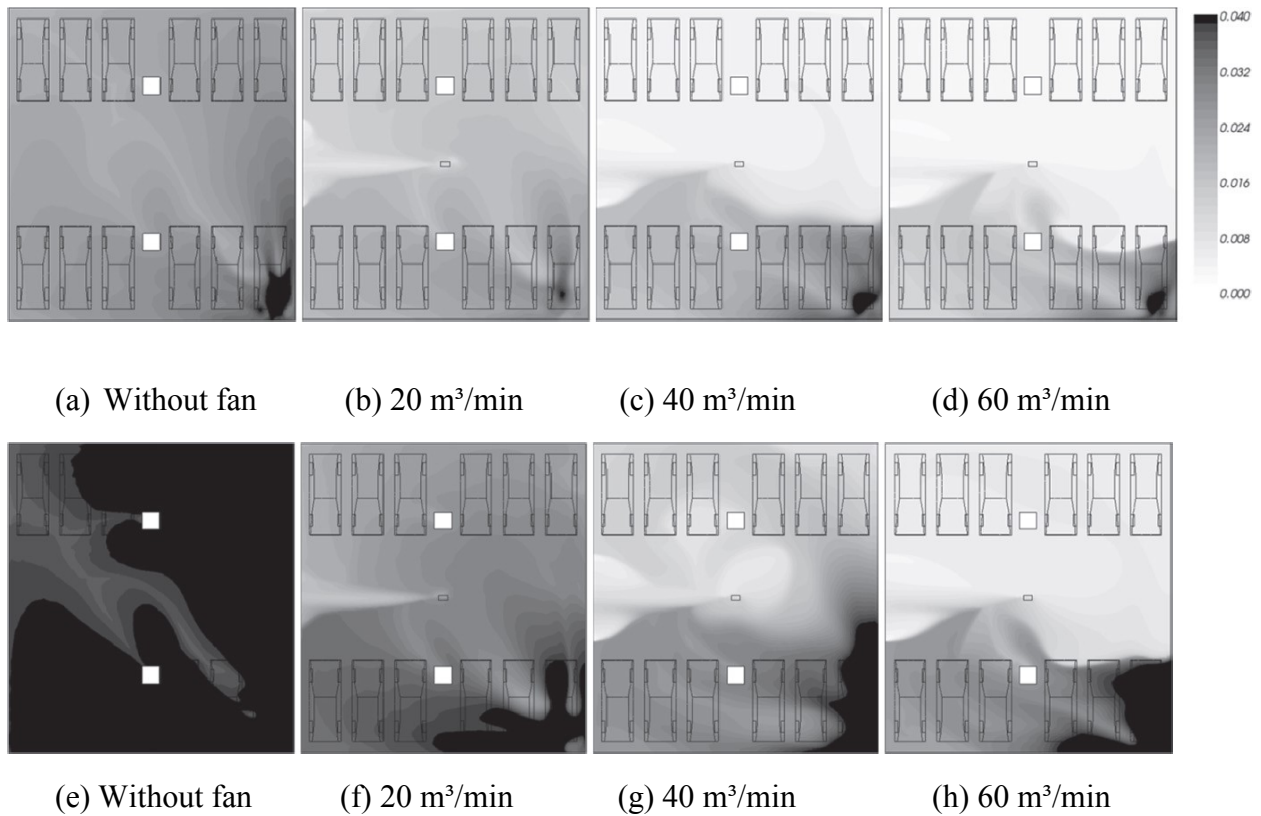
Figure 1.7 Contours of the volume fraction of hydrogen air the ceiling for different ventilation air volumes. Leakage flow rate is $5Q$ for (a)~(d) and $10Q$ for (e)~(h) at 10 minutes

Choi et al. also compared the contours of hydrogen concentration at the ceiling for the cases with different air volumes by a ventilation fan and the case without a fan. It is obvious that as the air volume of the fan increases, the flammable region reduces. Near the boundary of the flammable region has larger gradient of the volume fraction as the air volume of fan increases. It is indicated that the ventilation fan plays an important role in enhancing mixing and delays the expansion of the flammable region [22]. Results in this study show the effectiveness of a ventilation fan to avoid a hazardous scenario from hydrogen leakage in an underground parking garage.

1.5   Research objectives

A number of literatures can be found using helium to understand the dispersion behavior of hydrogen and together with CFD software to predict the concentration of hydrogen. In the NIST tests, helium dispersion was studied in partially confined spaces and results were compared with FDS predictions. In the study of Swain et al., a new method called HRAM was proposed to evaluate hydrogen gas leaks using a CFD model which has been verified using helium leakage and concentration data. In the study of hydrogen leakage in underground parking garage, numerical results evaluate the effect of ventilation fan to relieve accumulation of hydrogen gas and decrease the expansion of flammable region.

In this thesis, three theoretical relationships for the similarity between hydrogen and helium are assessed using the validated CFD model. The accuracy of those different methods at different stages of release and location is discussed. And a new updated theoretical plume model was proposed and validated by Particle Image Velocimetry (PIV) experiment. Furthermore, a numerical study is performed to analyze hydrogen safety inside a fuel cell vehicle resulted from a hydrogen storage leakage. The effect of ventilation and sunroof on hydrogen dispersion are compared in different scenarios.

Specifically, the research objectives of this thesis are:

- To assess different theoretical relationships for the similarity between hydrogen and helium leakage in an enclosure.
- To provide a guide when using helium experiment to validate hydrogen simulation in different scenarios which is of importance to the investigation of hydrogen safety.

- To develop an updated theoretical model for a point source plume to predict the velocity and width of the ideal plume.

  With this theoretical model, vertical velocity of mixture and plume width could be directly calculated according to the volume flow rate of the leakage.

- To analyze the effect of ventilation and sunroof on hydrogen dispersion in a fuel cell vehicle.

1.6   Thesis outline

The structure of this thesis will be manuscript based.

Chapter 2 will be the paper "Assessment of similarity relations using helium for prediction of hydrogen dispersion and safety in an enclosure". A CFD model is built and validated using the helium data. Three relations are studied for the similarity between hydrogen and helium leakage.

Chapter 3 will be the paper "An updated helium plume model validated by PIV experiment". The detailed derivation of the equations are presented. Results of simulation, PIV experiments and theoretical calculations are compared.

Chapter 4 will be the paper "The effect of ventilation and sunroof on hydrogen dispersion in a fuel cell vehicle". Numerical model and simulation details are shown in this chapter. Results of hydrogen concentration in different scenarios are evaluated. A resolution study is also included in this chapter.

Chapter 5 presents the conclusions and suggested future work.

2 Assessment of similarity relations using helium for prediction of hydrogen

2.1 Theory

From the previous work by Swain et al. [23] where the hydrogen risk assessment method (HRAM) is introduced, it shows that, in simple geometric enclosures, helium can be used to simulate leakages of hydrogen and to predict the hydrogen concentrations near the ceiling. The method to assess the risk of hydrogen leakage relies on a CFD model calibrated by the data from helium experiments. The similarity between hydrogen and helium is obtained based on $Q_{H2} = Q_{He}$, where Q_{H2} and Q_{He} are volumetric flow rates of hydrogen and helium, in m³/s, respectively. Most current studies using helium as a surrogate to validate hydrogen simulation models are also formulated by assuming the same volumetric flow rate of both gases. Nevertheless, Swain et al. [24] observed that, before the plume becomes stable during the development stage, the helium concentration can be significantly different from that of hydrogen using the aforementioned analogy.
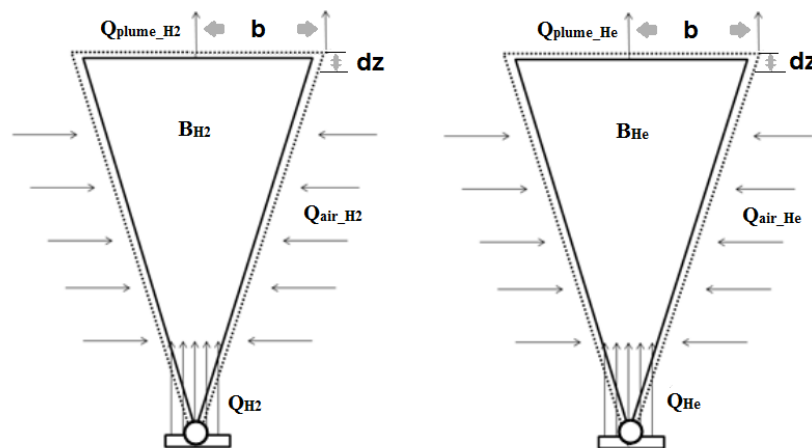

Figure 2.1 Schematics of the hydrogen and helium plumes

In order to use helium accurately as a surrogate gas for hydrogen, it is necessary to assess the similarity between the hydrogen and helium plumes. Inspired by the ideal plume theory in the field of fire science [25], the ideal plume models of hydrogen and helium can be developed as shown in Fig 2.1. Similar to that of a fire plume, the buoyancy flux of a buoyant gaseous plume, B in m^4/s^3, can be defined by:

$$B = gQ_{gas}\left(\frac{\rho_{air} - \rho_{gas}}{\rho_{air}}\right) \tag{2.1}$$

where ρ_{air} is the surrounding air density in kg/m^3, g is the acceleration of gravity, in m/s^2, and Q_{gas} is the volumetric flow rate of the plume, in m^3/s. In this study the temperature is assumed to be constant in the plume and in the ambient air and thus, the difference of density is caused by a scale factor, which is a function of the height z. The volumetric flow of the gas Q_{gas} is also kept constant. The volumetric concentration, C, is then given by:

$$C = \frac{Q_{gas}}{Q_{plume}} = \frac{Q_{gas}}{\pi b^2 u} \tag{2.2}$$

b is the radius of the plume, u is the upward gas velocity. The density and the mass flow rate of the plume are thus:

$$\rho_{plume} = C\rho_{gas} + (1-C)\rho_{air} = \rho_{air} + \frac{Q_{gas}}{\pi b^2 u}\left(\rho_{gas} - \rho_{air}\right) \tag{2.3}$$

$$\dot{m}_{plume} = Q_{plume}\rho_{plume} = \pi b^2 u \rho_{plume} \tag{2.4}$$

The ambient air is assumed to entrain at a rate proportional to the plume velocity u, i.e., $v = \alpha \cdot u$, where α is referred to as the entrainment ratio. By equating the rate of mass change over the height dz and the rate of air entrainment through the sides of dz satisfying the conservation of mass, it yields:

18

$$\frac{d\dot{m}_{plume}}{dz} = \frac{d(\pi b^2 u \rho_{plume})}{dz} = \frac{2\pi b u \alpha \rho_{air} dz}{dz}$$

$$\frac{d(b^2 u \rho_{plume})}{dz} = 2 b u \alpha \rho_{air} \tag{2.5}$$

Similarly, by equating the rate of momentum change over height dz and the differential buoyancy force acting on the mass within height dz based on the conservation of momentum, the following expression is obtained:

$$\frac{d(\dot{m}_{plume} u)}{dz} = \frac{dF}{dz}$$

$$\frac{d(\pi b^2 u^2 \rho_{plume})}{dz} = g(\rho_{air} - \rho_{plume})\pi b^2 \tag{2.6}$$

Solving the two combined differential equations above, it gives:

$$C(z) = \frac{Q_{gas}}{Q_{plume}} = \frac{Q_{gas}}{\pi b^2 u} = \frac{Q_{gas}}{\pi \frac{36}{25}\alpha^2 \left[\frac{25 B_{gas}}{48\pi\alpha^2}\right]^{1/3} z^{5/3}} \tag{2.7}$$

In order to obtain the same concentration level for both hydrogen and helium,

$$C_{H2}(z) = C_{He}(z)$$

$$\frac{Q_{H2}}{\pi \frac{36}{25}\alpha^2 \left[\dfrac{25 g Q_{H2}\left(\dfrac{\rho_{air} - \rho_{H2}}{\rho_{air}}\right)}{48\pi\alpha^2}\right]^{1/3} z^{5/3}} = \frac{Q_{He}}{\pi \frac{36}{25}\alpha^2 \left[\dfrac{25 g Q_{He}\left(\dfrac{\rho_{air} - \rho_{He}}{\rho_{air}}\right)}{48\pi\alpha^2}\right]^{1/3} z^{5/3}} \tag{2.8}$$

After some mathematical manipulation, the following relationship can be obtained:

$$Q_{He} = Q_{H2}\sqrt{\frac{(\rho_{air} - \rho_{He})}{(\rho_{air} - \rho_{H2})}} \tag{2.9}$$

Using the above correlation, for any given hydrogen volumetric flow rate, the helium volumetric flow rate can be calculated which gives the exact concentration level as hydrogen, or vice-versa.

For fire science applications, it is common to maintain a same buoyancy flux to ensure the dynamical similarity of plumes [26-28]. Similarly, it is also possible to come up with another correlation based on the equal buoyancy flux of the two gases:

$$B_{He} = B_{H2} \qquad\qquad (2.10)$$

and it gives:

$$Q_{He} = Q_{H2} \frac{(\rho_{air} - \rho_{He})}{(\rho_{air} - \rho_{H2})} \qquad\qquad (2.11)$$

Combine the above two correlations into one, a generalized expression can be obtained as:

$$Q_{He} = Q_{H2} \left[\frac{(\rho_{air} - \rho_{He})}{(\rho_{air} - \rho_{H2})} \right]^n \qquad\qquad (2.12)$$

When $n = 1/2$, the correlation is based on equal concentration as derived in this section (Method A); For the $n = 0$, the above equation reduces to the equal volumetric flow rate (Method B or equivalently the HRAM method); and finally, the equal buoyancy model is yielded with $n = 1$ (Method C).

2.2 Numerical simulation

2.2.1 Numerical modeling of reduced scale experiments with helium

In this study, the CFD simulations were divided into two stages. The chosen CFD model was first validated with experimental data of helium release in the scaled enclosure, see Fig. 2.2a. Simulations of hydrogen dispersion were then conducted using the validated CFD model and the results were used to assess the similarity models described in Sec. 2.2.2.
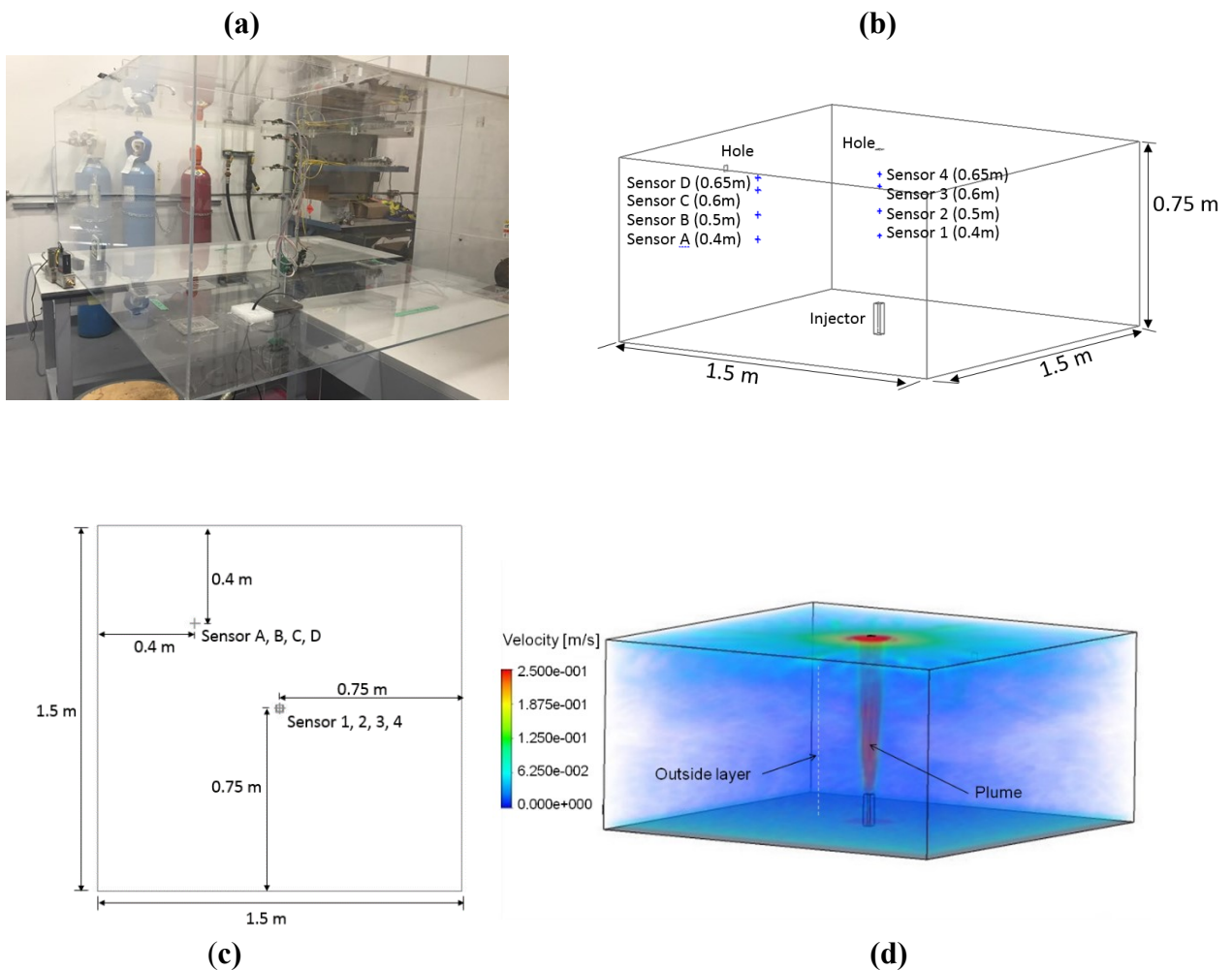
(a)
(b)

(c)
(d)

Figure 2.2 Photograph of the experimental setup, and a schematic of the computational domain and a sample velocity contour plot

The experiment is conducted by Kokgil [26]. For the experiment, a 1.5 m × 1.5 m × 0.75 m with 0.6-cm-thick chamber made of Plexiglas was built, representing a 1:4 scaled two-car residential garage. An injector was used to release the helium into the chamber. The injector was 12.5 cm tall and the inlet size was 36 mm × 36 mm. A uniform room temperature of 21°C is expected to maintain at the exit section. A mass flow controller adjusted the helium flow at 15 L/min (a typical hydrogen leakage rate for hydrogen storage tanks is 1 to 15 L/min). Several small vents were chosen to provide minimum ventilation requirements for residential garages, of 3 air changes per hour (ACH) [13]. The vents consist of single 2.6-cm-square openings at the center of the ceiling and at the top of the side faces. For the case of forced ventilation, the boundary condition in the ceiling vent was changed to a ventilation fan with 4.2 CFM (from the ASHRAE standard [13]). Helium concentrations were measured with eight sensors, at two horizontal locations (i.e., one at 40 cm from the side and the front, and the other at the floor center). Sensors 1 to 4 and sensors A to D were located inside and outside the plume, respectively. Each set of sensors were mounted 0.4, 0.5, 0.6 and 0.65 m above the floor, see Figs. 2.2b and 2.2c.

The commercial software ANSYS FLUENT [29] was used in this study for all simulation cases. The geometrical model utilized within the CFD is equivalent to that of the present reduced, scaled experiment with helium, as shown in Fig. 2.2b. A finite volume scheme with 2nd order accuracy was used to discretize the governing Navier-Stokes equations. A Large Eddy Simulation (LES) was applied as the turbulence model, and the PISO-SIMPLE (PIMPLE) algorithm with a time step size Δt of $4 \times 10^{-7} \sim 5 \times 10^{-7}$ for obtaining a stable solution to the discretizing equations [30-31]. All the numerical simulations were performed using the computer cluster available at the High Performance Computing Virtual Laboratory (HPCVL) managed by Compute Canada [32]. The simulations were performed using similar initial conditions as in the experiment with a leak source

located close to the floor in the garage. The leak area was 3.15 cm $\times$ 3.15 cm and the mass flow rate of the leak was 4.178 x 10^{-5} kg/s. Both the initial temperature of released helium and air temperature in the chamber were set equal to 297 K and initial pressure to 101 kPa. For the ceiling vent a pressure outlet boundary condition was used; while for side wall vent velocity inlet was used. The gas injection was modeled using a mass flow inlet boundary condition. A structured grid made of rectangular cells was used for meshing. Unless specified, the mesh size varies from 0.004 m close to the injector to a maximum value of 0.016 m. 484,166 grid cells in total were contained in the computational model. A resolution study was indeed carried out and found that an increase in the current grid resolution has only a negligible effect on the concentration levels. Figure 2.3 shows the simulated results measured by sensors 1 and 4 inside the plume, and by sensors A and D for the layer outside the plume with three different mesh resolutions. It is found that an increase of the total mesh number by 10%, i.e., from 484,166 to 523,580 grid cells, results in a percentage difference less than 1% in the overall change of helium concentrations.
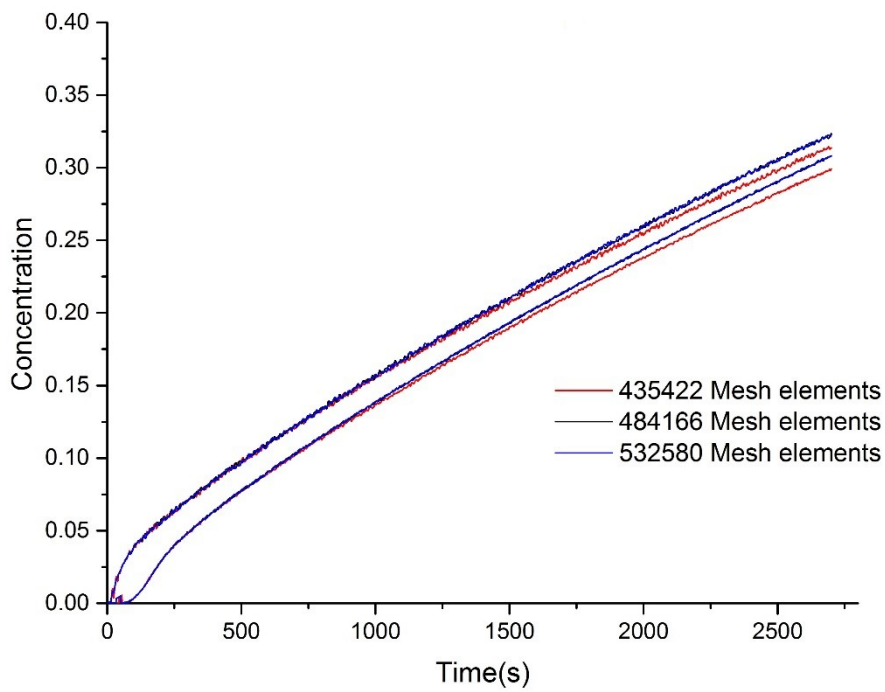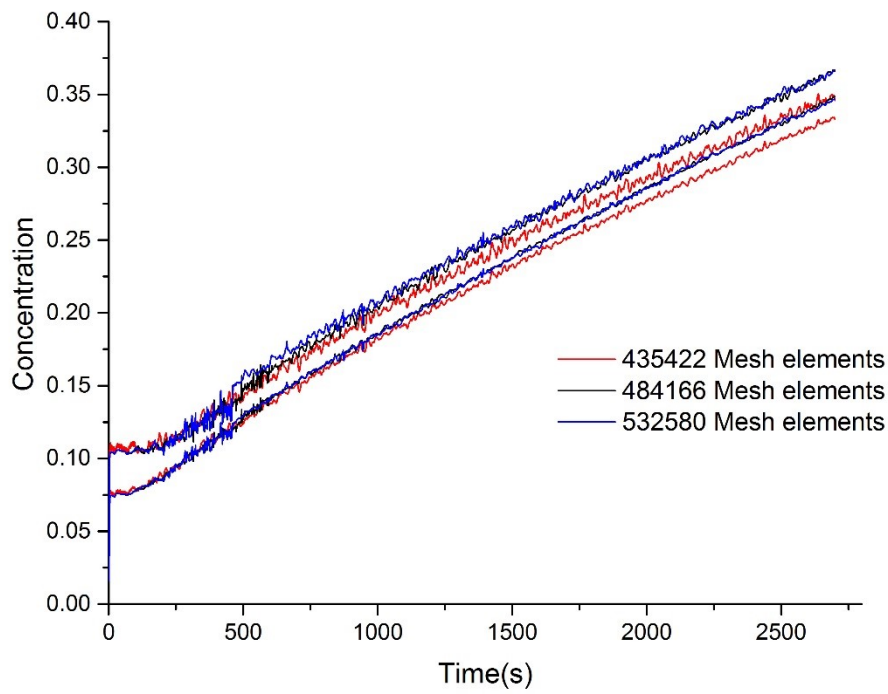
Figure 2.3 Effect of changing the mesh elements number on the helium concentration for a) inside the plume (Sensor 1 and 4); and b) at the layer outside the plume (Sensor A and D)

Figure 2.4 compares the evolution of helium concentration obtained from both the experimental measurement (given by discrete points) and CFD numerical simulation (represented by solid lines). Simulation time for this validation case lasts for 2,700 s. Overall, both results agree reasonably well with each other. The average percentage difference of the simulation results to experiment data for all sensors is 7.6%. Both results also show that the sensors inside the plume (Sensors 1 and 4) records accordingly higher concentrations than those obtained for sensors A-D in the layer region outside the plume.

Figure 2.4 Comparison of experimentally measured helium concentration (points) with simulation values (lines) obtained by two sets of sensors located at various heights

2.2.2 Simulations of hydrogen leakage

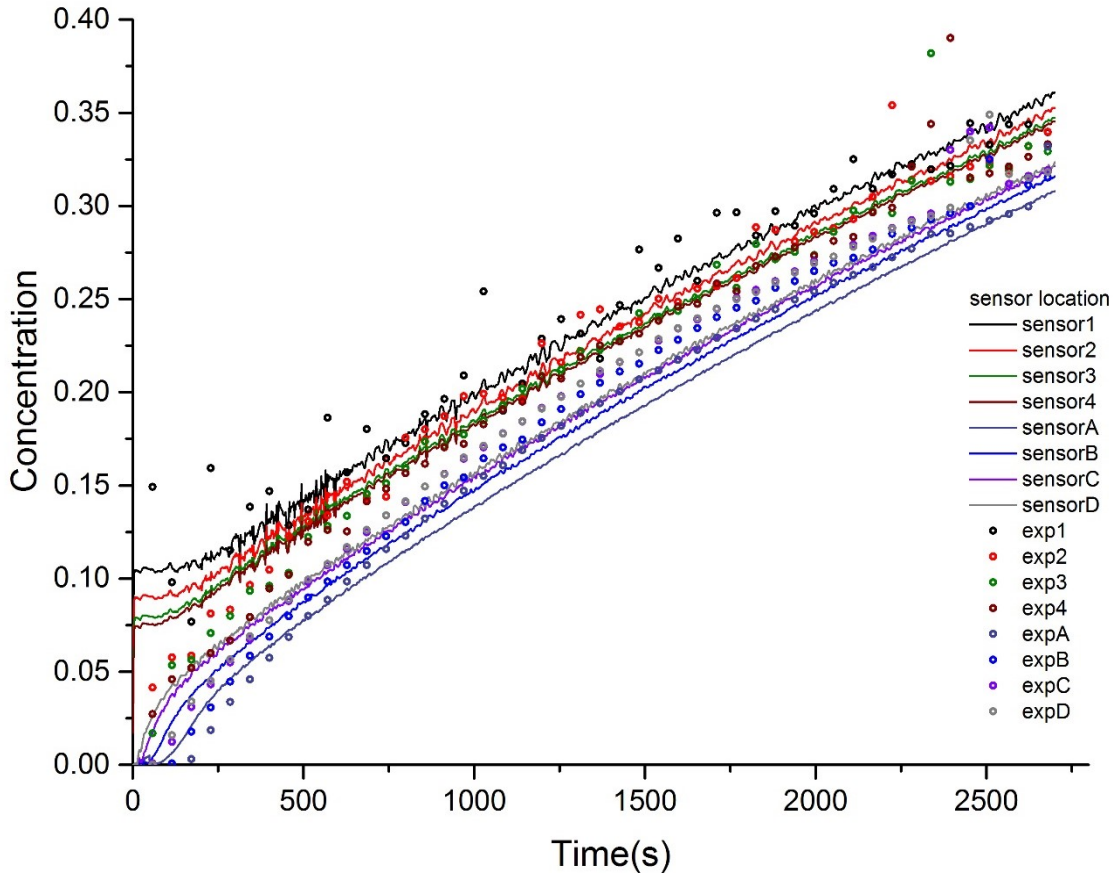The same CFD model validated in the above section is used to simulate the hydrogen dispersion in the same computational setting, with the physical property values for hydrogen instead of those for helium. To evoke the similarity, the equivalent hydrogen volumetric flow rate is determined using Eq 2.12 with different n, giving the various correlation based on the newly proposed correlation obtained with equal concentration, equal volume flow rate and equal buoyancy with values of 15.6 L/min, 15.0 L/min and 13.88 L/min, respectively.

Table 2.1 Time-averaged percentage difference of hydrogen concentration relative to helium from 0 to 2,700 s

	Sensor 1, 2, 3 and 4 (inside plume)	Sensor A, B, C and D (outside layer)
Method A	4.4%	4.1%
Method B	5.5%	1.8%
Method C	6.5%	7.6%

Figures 2.5 and 2.6 compare the numerical results for the evolution of helium and hydrogen concentrations, obtained based on the three similarity models. It is found that there is noticeable difference in the results obtained at different regions, i.e., inside the gas plume or outside the plume. Figure 2.5 shows the concentration results measured by the sensors 1 and 4 inside the plume which represents the high risk domain in hydrogen leakage. A large flow fluctuation also resulted inside the plume as shown in Fig. 2.5. In all cases, the graphs show that hydrogen has a similar tendency with helium with small difference. Because simulated helium data is validated by experiment, so we define the percentage difference as: $(C(\text{He}) - C(\text{H}_2))/C(\text{He}) \times 100\%$ for a

26

quantitative comparison, it is found that the time-averaged percentage differences from all sensors measurement for Method A, B and C are 4.4%, 5.5% and 6.5%, respectively (see also Table 2.1). The concentration levels outside the plume are presented in Fig. 2.6, and the results show less fluctuation than those in Fig. 2.5. Method B brings overall the minimum time-averaged percentage difference of 1.8%. In all cases, the average percentage differences obtained from the different methods are not pronounced, particularly if various uncertainties in the simulation (e.g., physical model, grid resolution, etc.) are taken into account. Hence, it is suggested that all three methods can be used when the region of interest is that inside the plume and for long time evolution at different layers outside the plume.
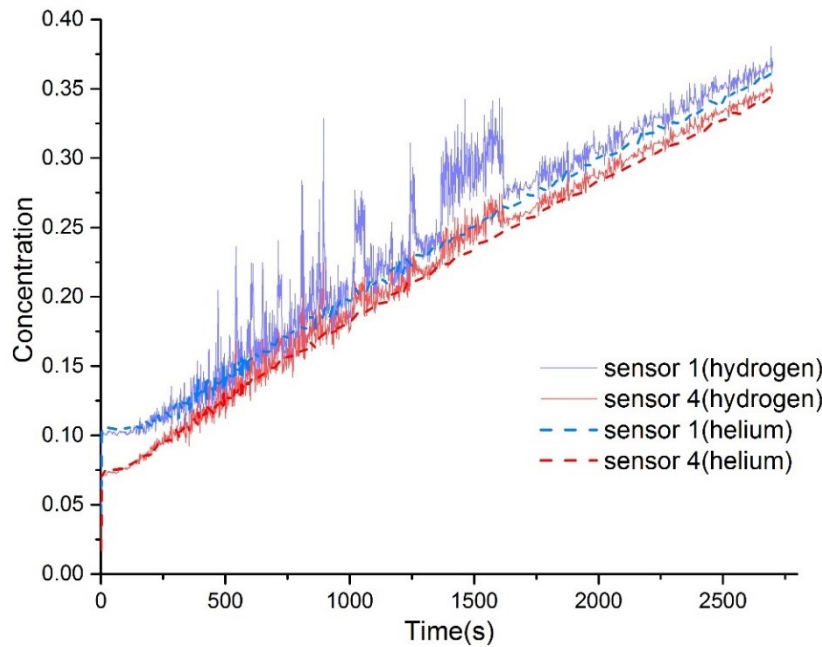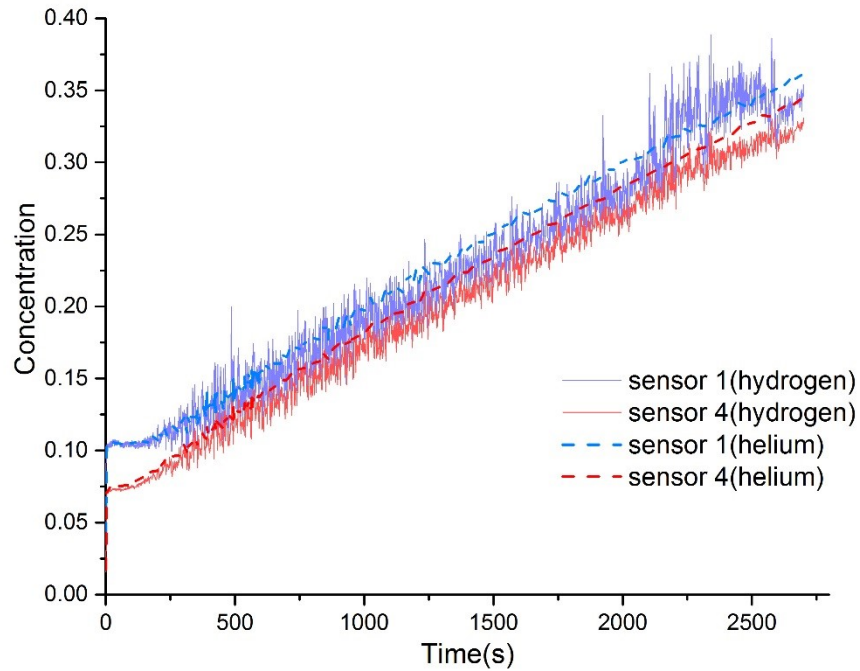

(a)

Figure 2.5 (continued)
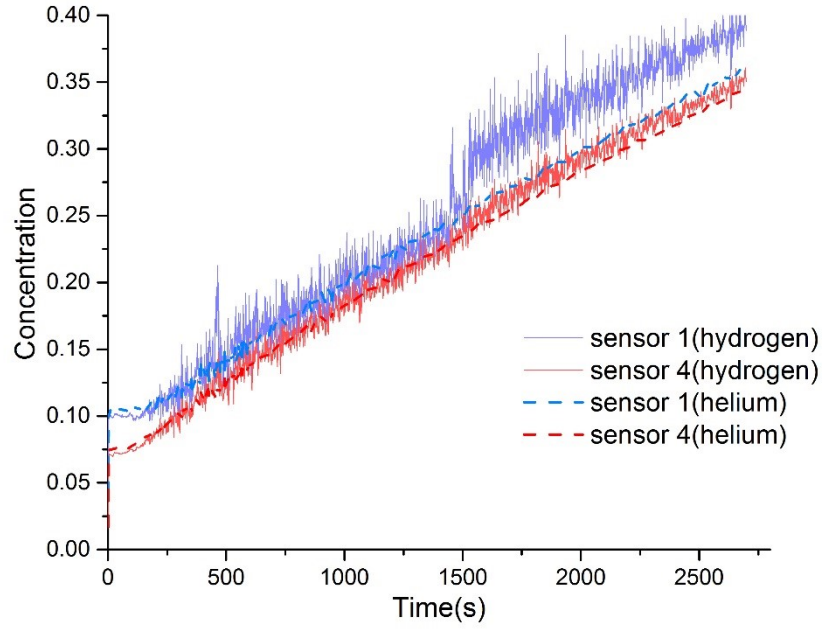
(b)

(c)

Figure 2.5 Comparison of simulated hydrogen concentration (solid line) inside the plume with the simulated helium results (dashed line) based on a) Method A; b) Method B; and c) Method C
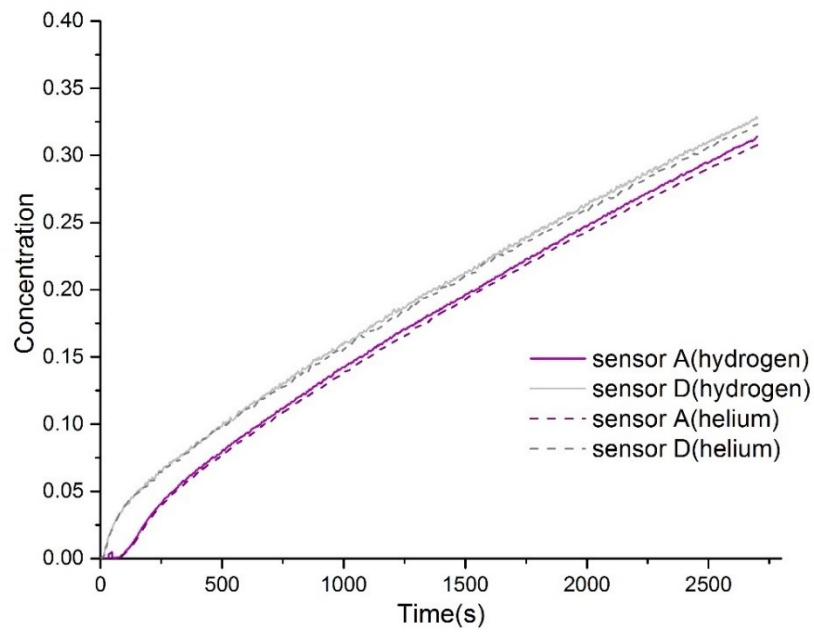
(a)
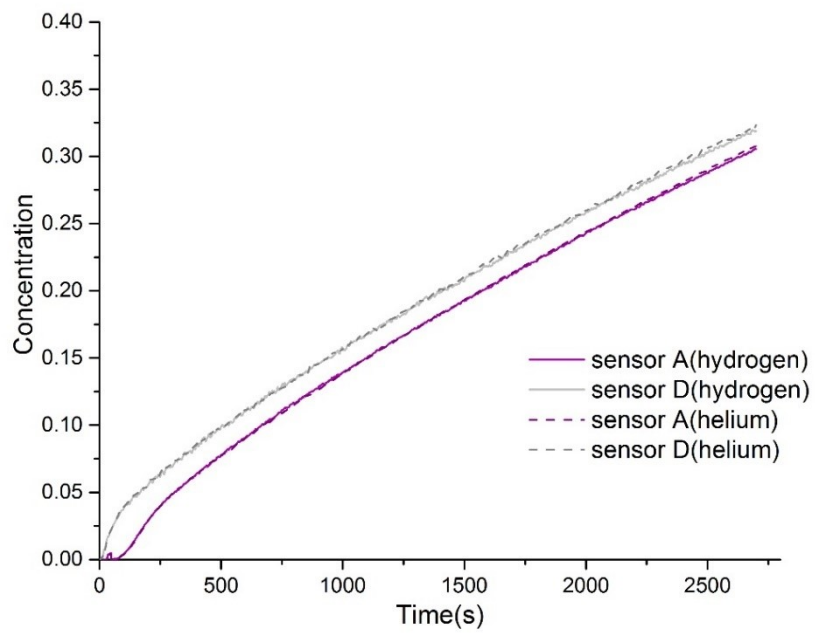
(b)

Figure 2.6 (continued)

(c)

Figure 2.6 Comparison of hydrogen concentration (solid lines) at the layer outside the plume with helium results (dashed line) based on a) Method A; b) Method B; and c) Method C

If the early stage of the release (i.e., less than 100 s) is of particular interest, however, Methods A and B might lead to a noticeable discrepancy. This result is indeed consistent with the finding by Swain et al. [21]. It is worth noting that based on the buoyancy effect Method C shows better similarity in the early stage of release (e.g., before 100 s) as shown in Fig. 2.7, except the measurement from the sensor D where the dispersion is influenced significantly by the near outlet located at the ceiling. Figure 2.7 also shows bumps in the initial stage of dispersion. At the very early instant, an increase of dispersed gas concentration accumulating in the ceiling is recorded by the sensors located at lower heights. As the surrounding air flows in through the outlet at the

30

sidewall, a decrease in the gas concentration is resulted due to the air entrainment and leading to the appearance of these bumpy behaviors of the results.

(a)

(b)

Figure 2.7 (continued)
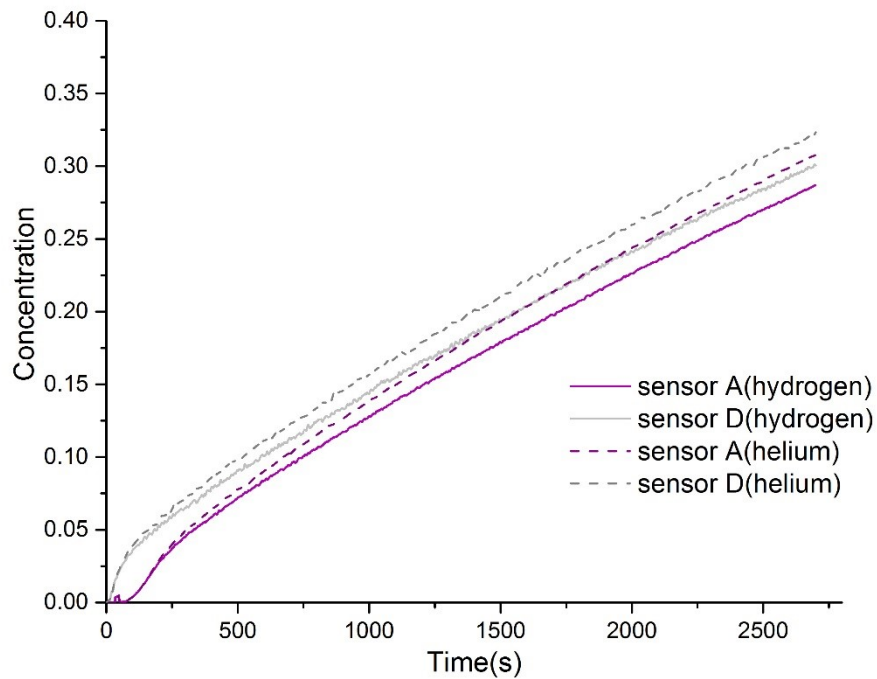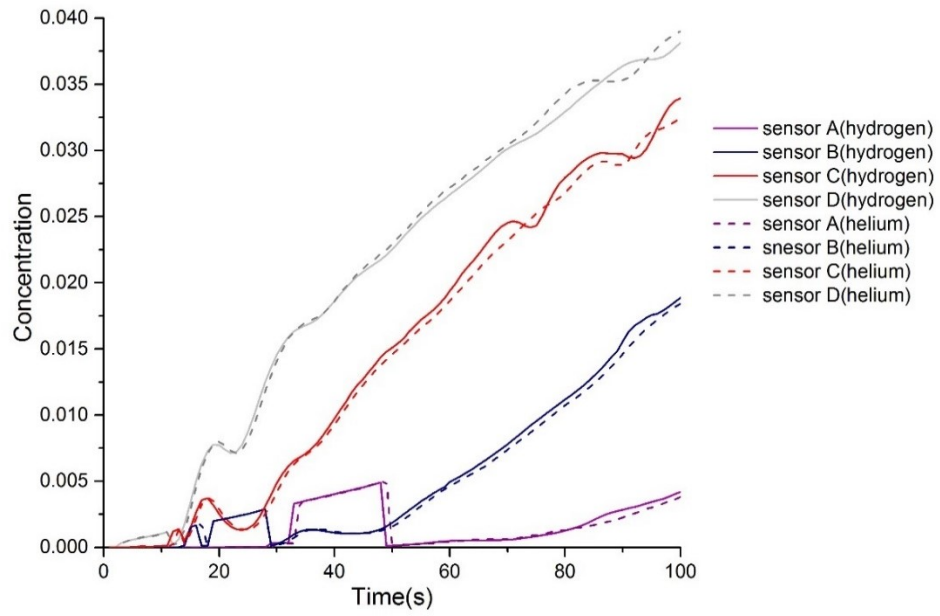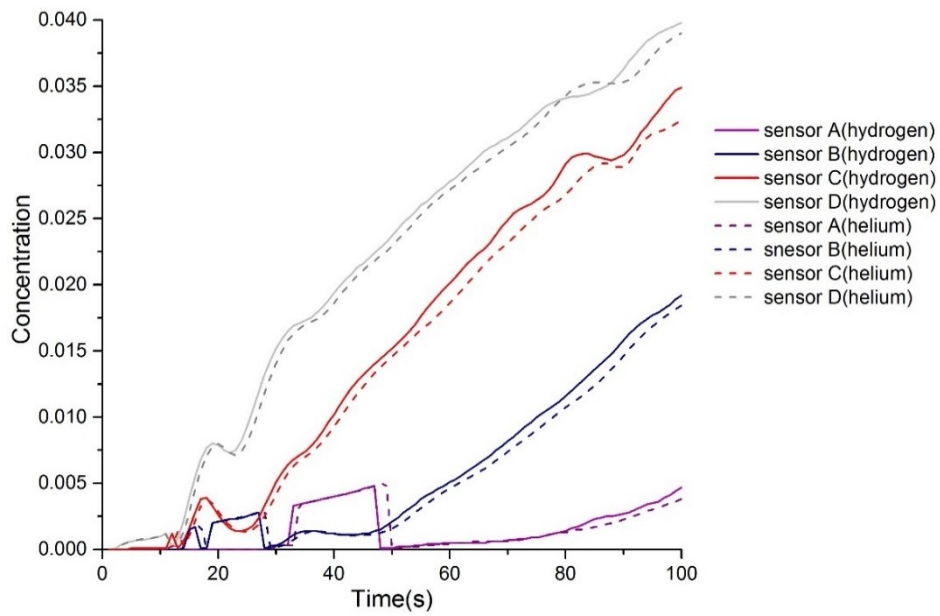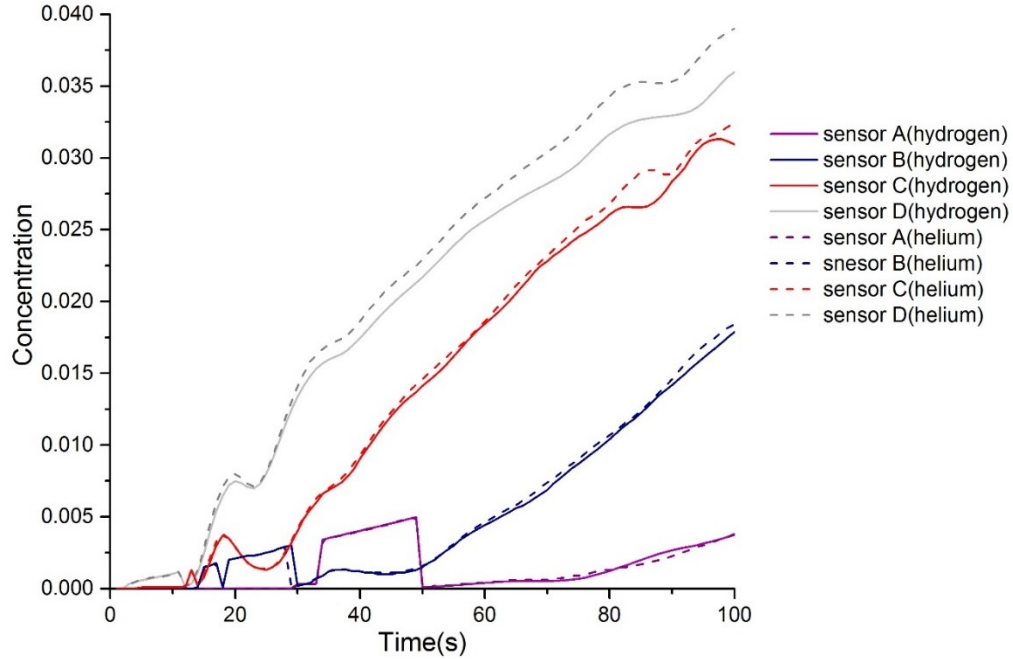
(c)

Figure 2.7 Comparison of hydrogen concentration (solid lines) at the layer outside the plume with helium results (dashed line) for the early release stage from 0 to 270 s based on a) Method A; b) Method B; and c) Method C

From the plume model [26, 27], buoyancy is the main controlling parameter on the velocity when considering the gas plume,

$$u(z) = \left[\frac{25 B_{gas}}{48 \pi \alpha^2} \right]^{\frac{1}{3}} z^{-\frac{1}{3}} \qquad (2.13)$$

It is worth noting that from the general transport equation, the gas release into the chamber is driven by both convection and diffusion mechanism [33]. From Eq. (2.13), equal buoyancy gives equal velocity which brings the same value of convection, while the value of diffusion is different. At the initial stage, the dispersion is driven mainly by convection. When the gas continuously diffuses into the chamber and accumulates at the upper layer leading to higher concentration

32

gradient, the effect of diffusion will start to play a dominant role at later dispersion evolution. Method C which is formulated based on the equal buoyancy between helium and hydrogen plumes give a more similar plume shape in the initial release and therefore, as shown in Fig. 2.7, has the better accuracy in the initial stage when the dispersion is convection-dominated.

A parametric study using different configurations by changing the injection height and volumetric flow rate was also performed to explore the accuracy of the three methods at the early stage of release from 0-100 s. It is indeed found that Method C always brings the least difference compared with the simulant (i.e., helium). For completeness, Figs. 2.8 and 2.9 present the results of these various parametric configurations obtained using the Method C to illustrate its accuracy at the early stage of release from 0-100 s.
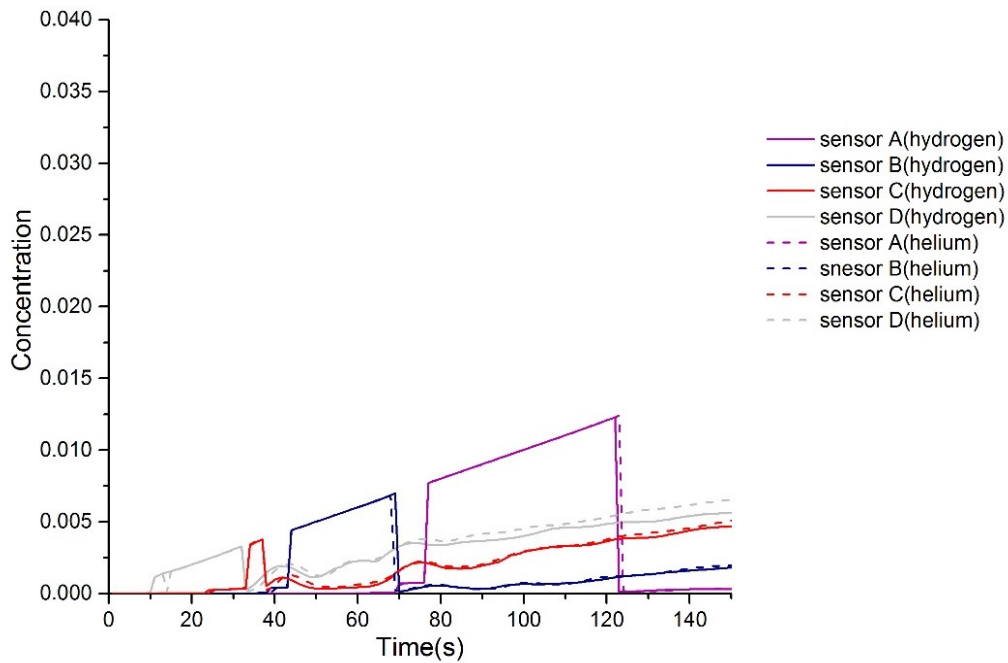
(a)

Figure 2.8 (Continued)

33
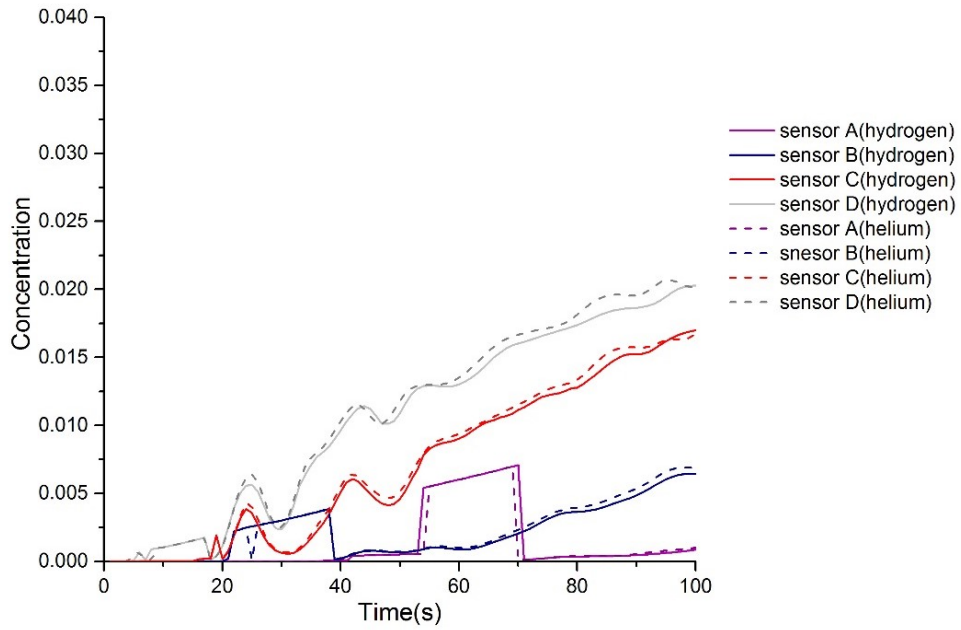
(b)
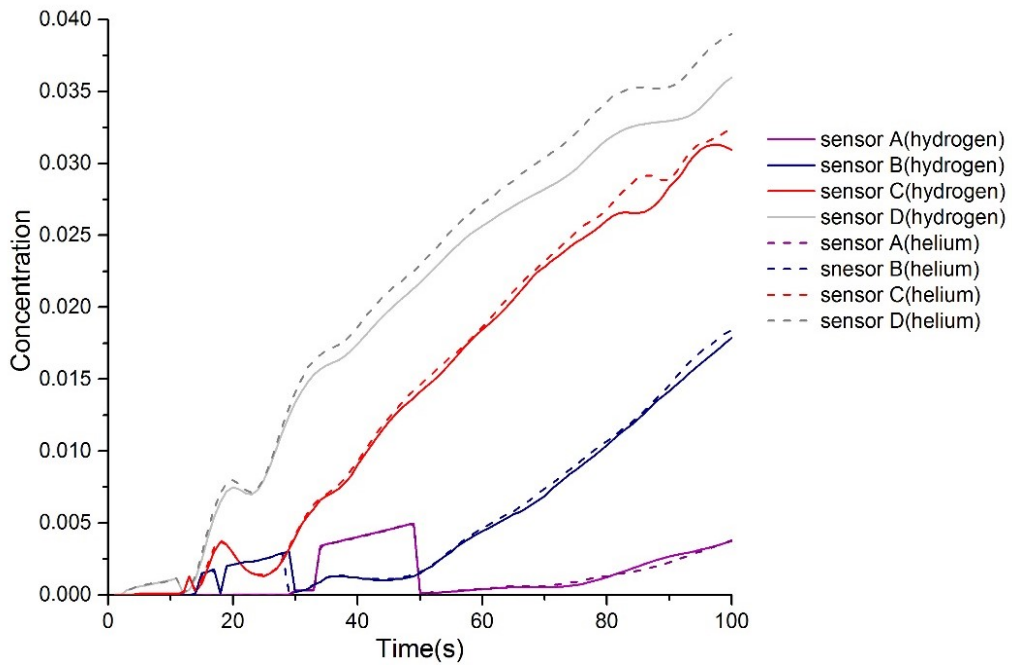
(c)

Figure 2.8 Comparison of hydrogen concentration results at the layer outside the plume based on method C (solid lines) with the helium results (dashed line) for different flow rates of a) 1.5 L/min; b) 7.5 L/min; and c) 15 L/min.
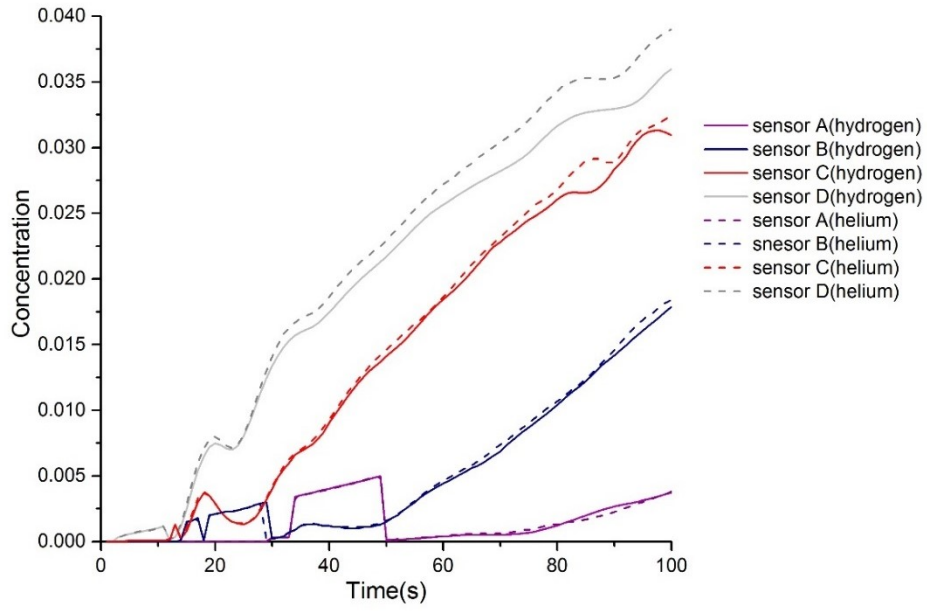
(a)
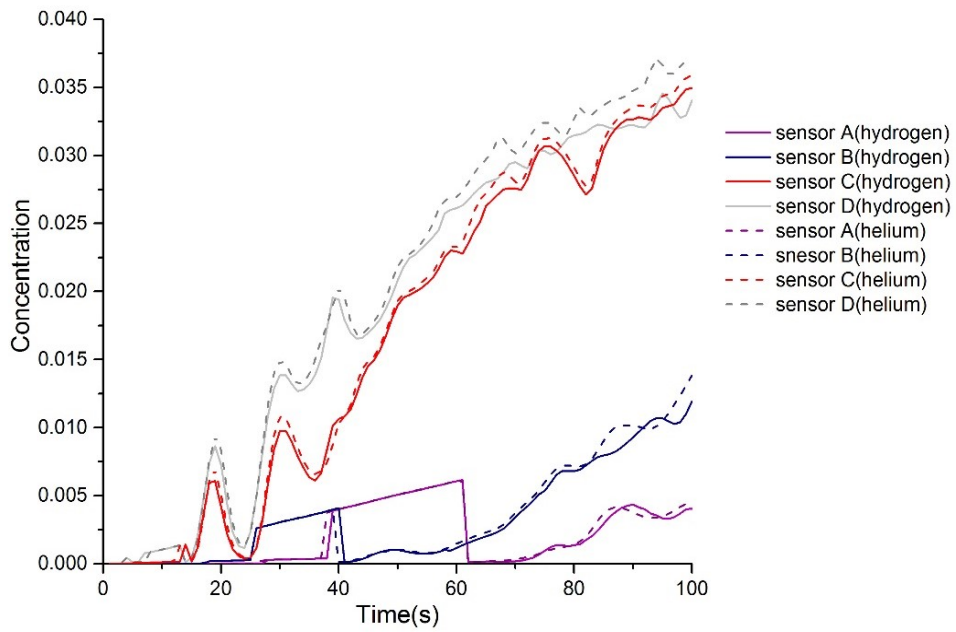
(b)

Figure 2.9 (continued)
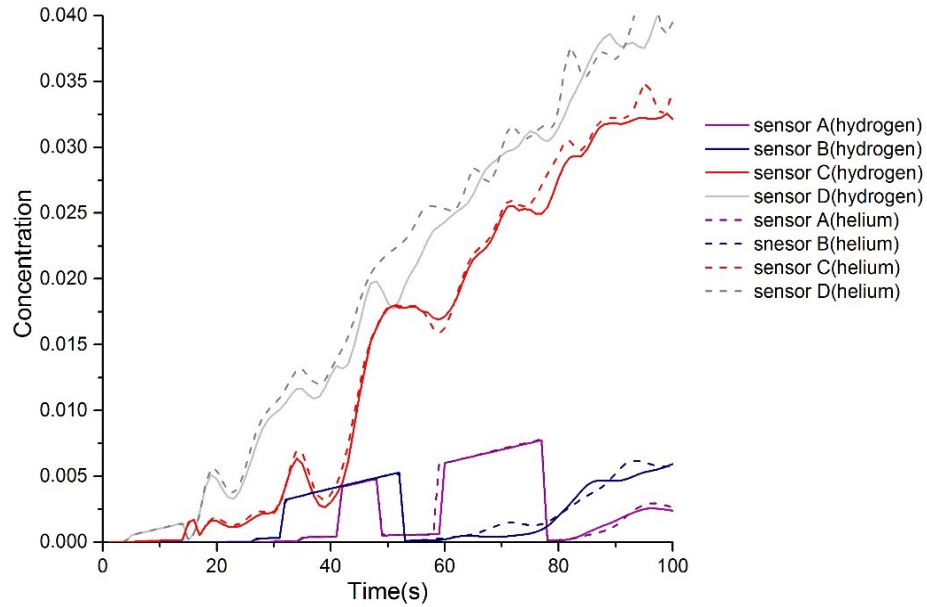
(c)

Figure 2.9 Comparison of hydrogen concentration results at the layer outside the plume based on method C (solid lines) with the helium results (dashed line) for injection heights of a) 12.5 cm; b) 35 cm; and c) 60 cm.

In the case with the inclusion of the mechanically driven flow, we consider the result in the outside layer region due to the significant fluctuation inside the plume as showed in Fig. 2.10, preventing any meaningful comparison. Fig. 2.11 compares the simulation results obtained based on Method A, B and C with helium in the outside layer. It can be observed that Method B presents the best correlation in Fig. 2.11 over the whole time interval from 0 to 2,700 s with a time-averaged percentage difference of 1.7% as compared to 11.3% and 7.0% determined for Method A and C, respectively. In the early stage, there is no huge difference for the reason that the ventilation fan weakens the plume effect, see Fig. 2.12. It is worth noting that the plume shape becomes stable at

a very short time. As a result, the improvement by using Method C is not as good as that in the case of natural ventilation.
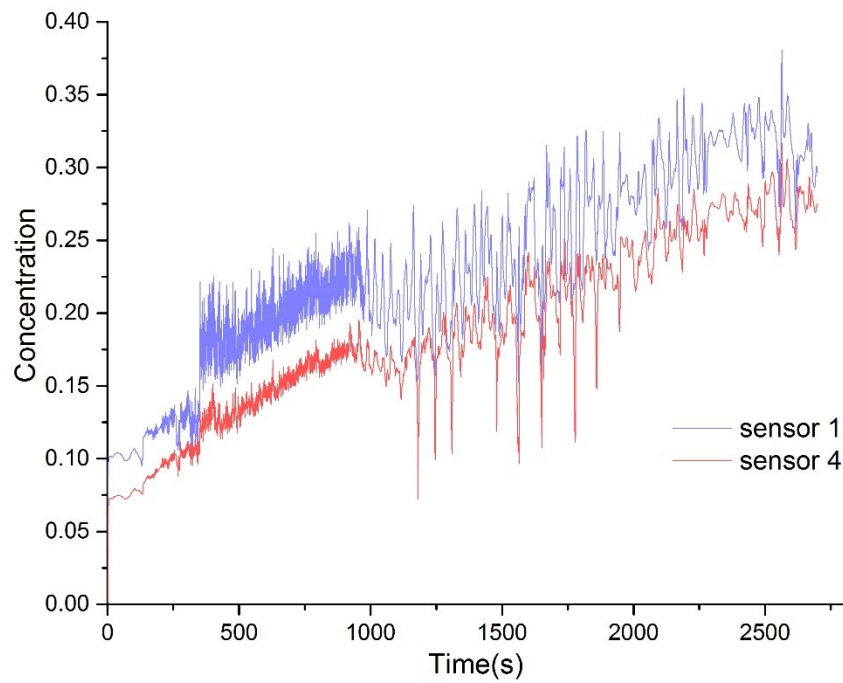
Figure 2.10 Simulation results inside the plume obtained using the Method A with forced ventilation
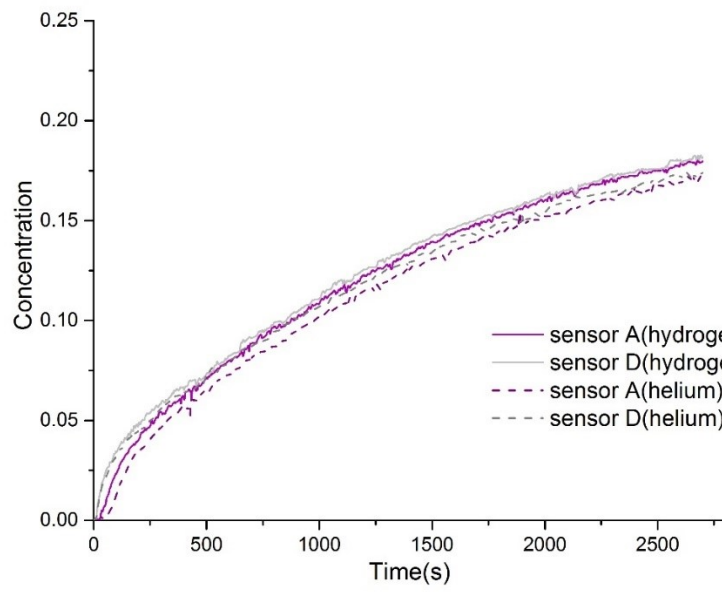
(a)
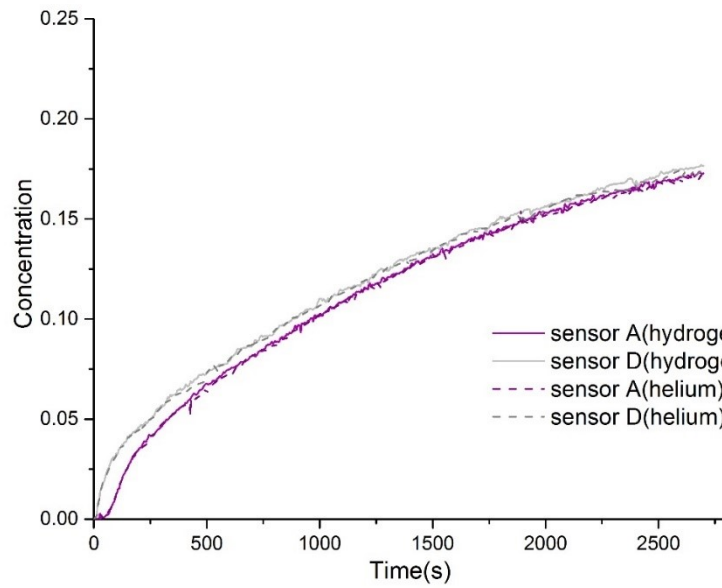
(b)

Figure 2.11 (continued)
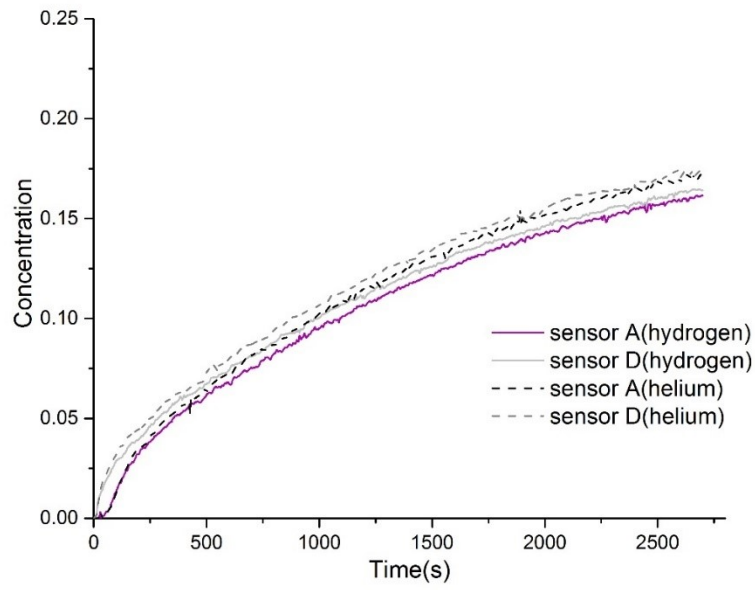
(c)

Figure 2.11 Comparison of hydrogen concentration (solid lines) at the layer outside the plume with helium results (dashed line) for the early release stage from 0 to 2700 s based on a) Method A; b) Method B; and c) Method C with forced ventilation

(a)

(b)
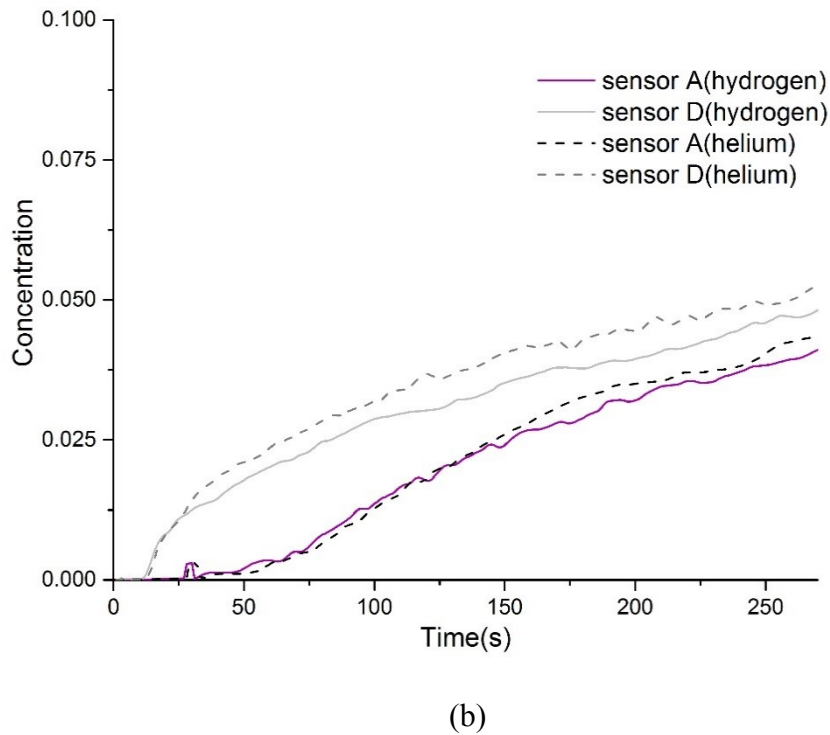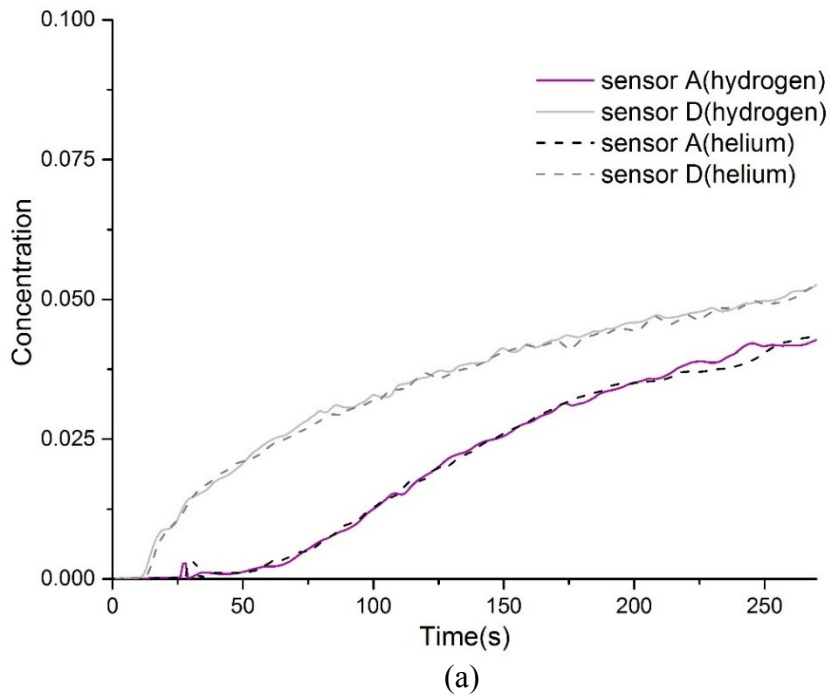
Figure 2.12 (continued)
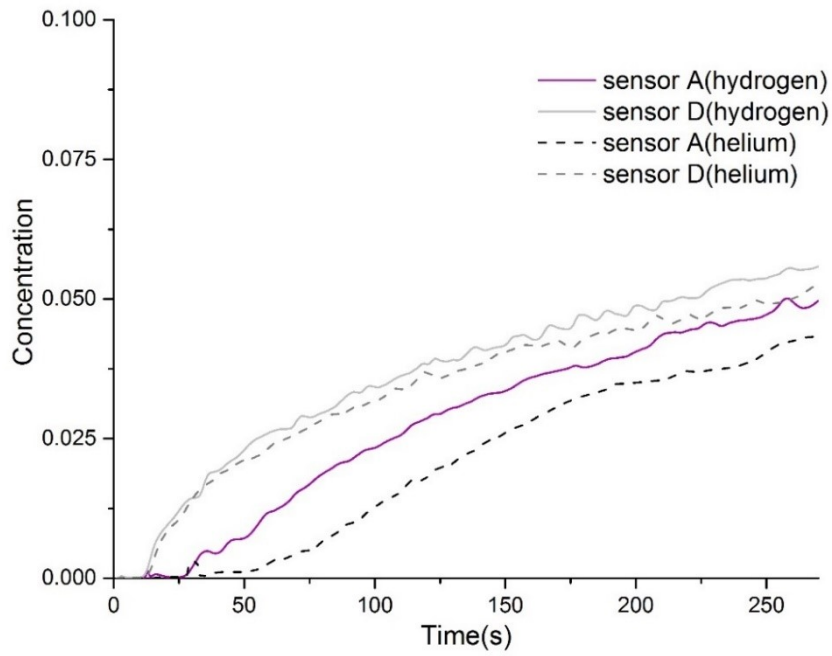
Figure 2.12 Comparison of hydrogen concentration plume (solid lines) at the layer outside the plume with helium results (dashed line) based on a) Method A; b) Method B; and c) Method C with forced ventilation

2.3 Summary

In the literature, helium is often used in experiments as a surrogate to stimulate hydrogen dispersion. In this work, three different relationships for the similarity between hydrogen and helium are reported and assessed using numerical simulations. Sub-scaled experiments measuring the helium concentration were used to validate the present CFD model. The same CFD model was then run with the physical property values for hydrogen instead of those for helium. The three correlations linking the helium with hydrogen based on equal concentration, equal volume flow rate and buoyancy were compared in the long-time release phase, early stage of release and the scenario with mechanical ventilation. If considering the overall time-averaged percentage difference inside the plume, the three methods give results close to each other. In the layer outside the plume, using the method of equal volumetric flow rate with helium gives the best overall results for the long-time release evolution. However, if the very early stage of release is of particular concern, the new proposed method of equal buoyancy (Method C) can improve the accuracy in multiple scenarios. While for the case of mechanical ventilation, the commonly used method (i.e., Method B) based on equal volumetric flow rate generally gives a reasonable similarity over the span of the release and at different regions. In this work, a detailed numerical investigation was conducted to highlight various possible similarity correlations to translate helium experiment into hydrogen simulation in different scenarios. The present results thus help to verify numerical approach in the study of hydrogen safety and the use of helium data for hydrogen dispersion analysis.

3 An updated helium plume model validated by PIV experiment

3.1 Introduction

Hydrogen presents a significant advantage for a renewable and environment-friendly energy carrier [1]. It can reduce public concerns related to pollutants and greenhouse gas emissions due to the exclusive reliance on fossil energy.

Substantial research and development have been developed in the hydrogen technologies related to production, storage and use of hydrogen. Due to the flammable properties of hydrogen, it is important to develop safety analysis [34]. Hydrogen is extremely flammable with in the concentration limits of 4-74% by volume in air, which can create safety challenges for public acceptance. Besides, hydrogen is the lightest gas and diffuses quickly, almost 3.8 times faster than natural gas and 2 times faster than helium [35]. The high buoyancy of hydrogen affects the movement of the gas even more than its high diffusivity. Because of these properties, hydrogen gas will disperse rapidly and form flammable mixtures with air when it leaks [16].

In the previous experiment studies, many researchers choose helium as a surrogate due to safety concerns for hydrogen. Swain et al. [23,24] showed that helium gas can be used to predict the distribution and concentration of hydrogen gas leakage scenario. This study provided a basis called Hydrogen Risk Assessment Method (HRAM) for predicting the concentration of flammable gases in enclosed space. HRAM utilizes the four steps: 1. Simulate the leakage scenario with helium; 2. Validate the CFD model of the leakage scenario using the helium experiment data; 3. Predict the results of hydrogen using the CFD model; 4. Identify the risk from the concentration and distribution of hydrogen.

Cariteau et al. [36] from Laboratoire d'Etude Experiméntal des Fluides, conducted experiments of simplified cases to investigate the dispersion behavior of hydrogen in confined spaces without ventilation. As in the previous experiment, helium was used as substitute of hydrogen due to safety reasons. Various configurations, where the source of the helium gas was jet or plume were studied. The aim was to quantify the effects of a leak from a fuel cell system within three different distinct regimes: stratified, stratified with a homogeneous upper layer and homogenous. This study cites that the magnitude of Richardson Number determines whether the flow is jet or plume.

He et al. [37] studied the theoretical analogy between helium and hydrogen in spatial and temporal distribution in the enclosure. Different correlations were compared at different periods of release, leakage rate, ventilation method and location. The correlations built a theoretical relationship between helium and hydrogen which is important to the study of hydrogen safety.

The above studies are mostly focused on the property of hydrogen or helium concentration. However, it has been proven that the spread velocity of gas and plume size are also crucial for the safety investigation [38]. The present study reports an analysis of a new helium plume model which can be used in estimating plume size and velocity. The model is validated by Particle Image Velocimetry (PIV) experiment and Computational Fluid Dynamics (CFD) simulations.

3.2 Theory

We compared the similarity between helium and hydrogen in our previous study [37]. It analyzed three different correlations between helium and hydrogen. It shows that helium can be used to replace hydrogen in experiment to predict the hydrogen concentration. Most of current studies focus on the properties of hydrogen and helium concentration. However, the size, geometry and spread velocity of the gas plume are also important for the hydrogen safety study. An estimation of the plume width and velocity can facilitate calculations on safety distance in hydrogen application, hydrogen leakage detection and analysis of flow field.

Inspired by the Heskestad Plume Theory [25], the previous ideal helium plume model [37] can be updated. The point source assumption is replaced by introducing a "virtual origin" at zero height.

With expressing the ideal plume properties, the following restricting assumptions need to be made:

1- The temperature is not changing in the plume or in the ambient air.

2- Ambient air is entrained at rate proportional to plume velocity, $v = \alpha u$.

3- The flow is similar in terms of velocity and density profiles at all heights. The difference occurs only by a scale factor, which is the function of height z.

4- Velocity and density are constant at each height.

5- Volumetric flow of the gas (Q_{gas}) is constant.

The plume of the light gas is considered as an upside down conical shape with a disc shaped element of height dz and radius b. Fig 3.1 represents the schematic of the plume of any light gas, where u is the plume velocity parallel to the flow axis in m/s.
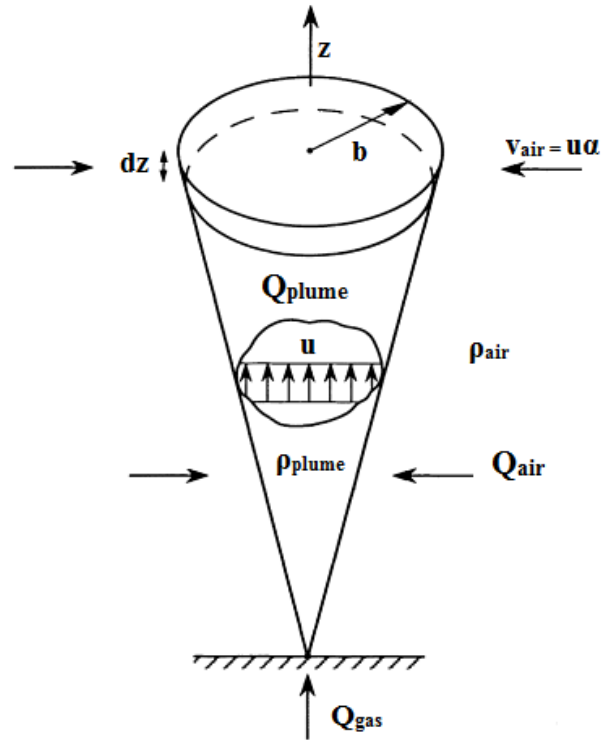
Figure 3.1 Schematic of light gas plume from a point source [37].

The density and the mass flow rate of the plume are:

$$\rho_{plume} = C\rho_{gas} + (1-C)\rho_{air} = \rho_{air} + \frac{Q_{gas}}{\pi b^2 u}\left(\rho_{gas} - \rho_{air}\right) \tag{3.1}$$

$$\dot{m}_{plume} = Q_{plume}\rho_{plume} = \pi b^2 u \rho_{plume}$$

where ρ_{air} is the surrounding air density in kg/m³, g is the acceleration of gravity, in m/s², and Q_{gas} is the volumetric flow rate of the plume, in m³/s. b is the radius of the plume, u is the vertical gas velocity

We can equal the rate of mass change over height

$$dz = \frac{d\dot{m}_{plume}}{dz} = \frac{d(\pi b^2 u \rho_{plume})}{dz}$$

46

and the rate of air entrainment through the sides of

$$dz = \frac{2\pi bu\alpha\rho_{air}dz}{dz}$$

according to the law of conservation of mass. Then we have Eq. (3.2)

$$\frac{d(b^2u\rho_{plume})}{dz} = 2bu\alpha\rho_{air} \qquad (3.2)$$

The rate of momentum change over height

$$dz = \frac{d(\dot{m}_{plume}u)}{dz} = \frac{d(\pi b^2 u^2 \rho_{plume})}{dz}$$

and the differential buoyancy force acting on the mass within height

$$dF = g(\rho_{air} - \rho_{plume})\pi b^2$$

should be equal according to conservation of momentum,

giving us Eq. (3.3)

$$\frac{d(\pi b^2 u^2 \rho_{plume})}{dz} = g(\rho_{air} - \rho_{plume})\pi b^2 \qquad (3.3)$$

By solving the two differential Eqs. (3.2) and (3.3),

the radius of the plume, b,

$$b(z) = \frac{6\alpha}{5}z \qquad (3.4)$$

And the velocity of the plume, u;

$$u(z) = \left[\frac{25 Q_{gas} g (\rho_{air} - \rho_{gas})}{48 \pi \rho_{air} \alpha^2} \right]^{\frac{1}{3}} \cdot z^{-\frac{1}{3}}$$

(3.5)

If we insert buoyancy flux in Eq. (3.5)

$$B = g Q_{gas} \left(\frac{\rho_{air} - \rho_{gas}}{\rho_{air}} \right)$$

We can express velocity of the plume:

$$u(z) = \left[\frac{25 B_{gas}}{48 \pi \alpha^2} \right]^{\frac{1}{3}} z^{-\frac{1}{3}}$$

(3.6)

This simplified model gives us a theory basis when buoyancy dominates in the gas flow. However, when we validate the plume model with simulation results, we find that the velocity, concentration and plume widths results are not well matched. It may be due to the fact that the inlet has width and initial velocity, the concentration distribution in certain height is not uniform, the surrounding gas is mixture and some air flows into the chamber through the outlet to keep the conservation of mass in simulation.

To overcome those problems, we can introduce a transformation in height.
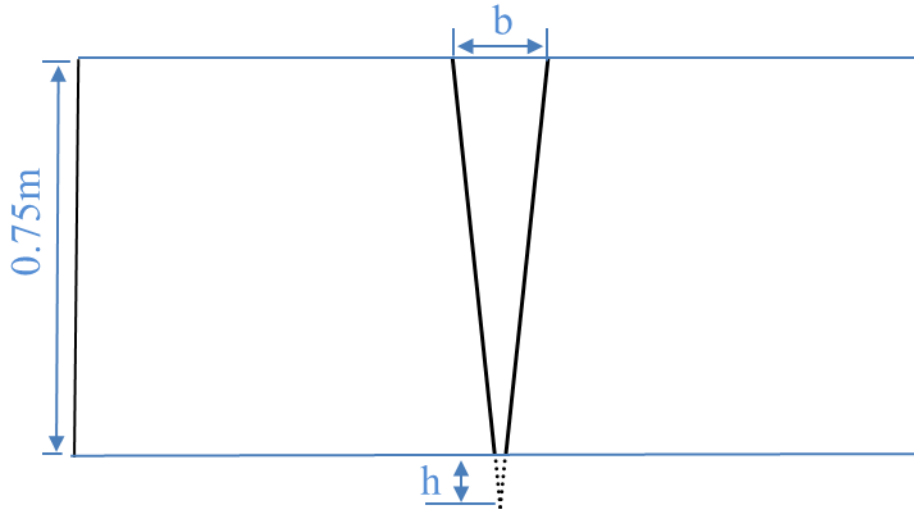
Figure 3.2 The new model adding a transformation in z direction

Here, b is the plume width, and h is the transformation. The vertical velocity in the inlet and the α

can be calculated by the following equation:

$$b(z) = \frac{6\alpha}{5}(z+h)$$

$$u(z) = \left[\frac{25B_{gas}}{48\pi\alpha^2} \right]^{\frac{1}{3}} (z+h)^{-\frac{1}{3}}$$

$$(3.7)$$

If the inlet is a circle whose radius is r, and we know the volume flow rate for helium is Q,

$$b(0) = 2r$$

$$u(0) = \frac{Q}{\pi \cdot r^2}$$

$$(3.8)$$

Combining Eqs. (3.7) and (3.8), and $B_{gas} = gQ_{gas}\left(\dfrac{\rho_{air} - \rho_{gas}}{\rho_{air}} \right)$,

$$h = \dfrac{Q^2}{\dfrac{9}{48} \cdot r^4 \pi^2 \left(g \dfrac{\rho_{air} - \rho_{he}}{\rho_{air}} \right)} \qquad (3.9)$$

3.3   Theory validation

In experiment and simulation, we set the inlet radius $r = 0.01$ m, volume flow rate $Q = 0.000125$ m³/s. From Eq. (3.8), we know that $h = 0.1$ m, $\alpha = 0.166$. Then we can use Eq. (3.7) to compare the velocity and plume widths results.

The same experiment chamber used in the previous study [37] was also used here, 1.5 m x 1.5 m x 0.75 m with 0.6 cm thick chamber made of Plexiglas. The diameter of the inlet was 0.02m. A mass flow controller adjusted the helium flow at 7.5 L/min. The initial air temperature in the chamber was set to 297 K and the air pressure to 101 kPa. Meanwhile, an outlet with the diameter of 18 cm was built in the ceiling (calculating from the theory part).

Particle Image Velocimetry (PIV) experiment is used to measure the real plume graph. Nd:YAG Laser system (New Wave Research Solo 120) equipped with light sheet optics (DANTEC 80×80 series) provides a laser light sheet system for visual inspection of plume width and velocity (see Fig. 3.3). The CCD camera – DANTEC Dynamics used in the experiment is a thermos-electrically cooled 14 bit camera with a 2M (1200 x 1600 pixels) resolution. The camera is equipped with a 60 mm lens (2.8/32, by Nikon). The commercial software, Flow Manager, provided image processing and analysis and was run on a 3.6 GHz dual processor workstation with 4GB of RAM, a 500 GB hard disk.

Aluminum oxide which is added into helium in a mixing box under the chamber is used as seeder in this experiment. The total release time is 300 s. Field of view in this experiment is 35 cm x 35

cm. The grid size in the PIV analysis 0.476 mm x 0.476 mm. The time interval, *dt*, between image pairs is 2.9×10^{-3} s. The displacement of particle in one time interval is less than one quarter of grid size.

(a)   (b)
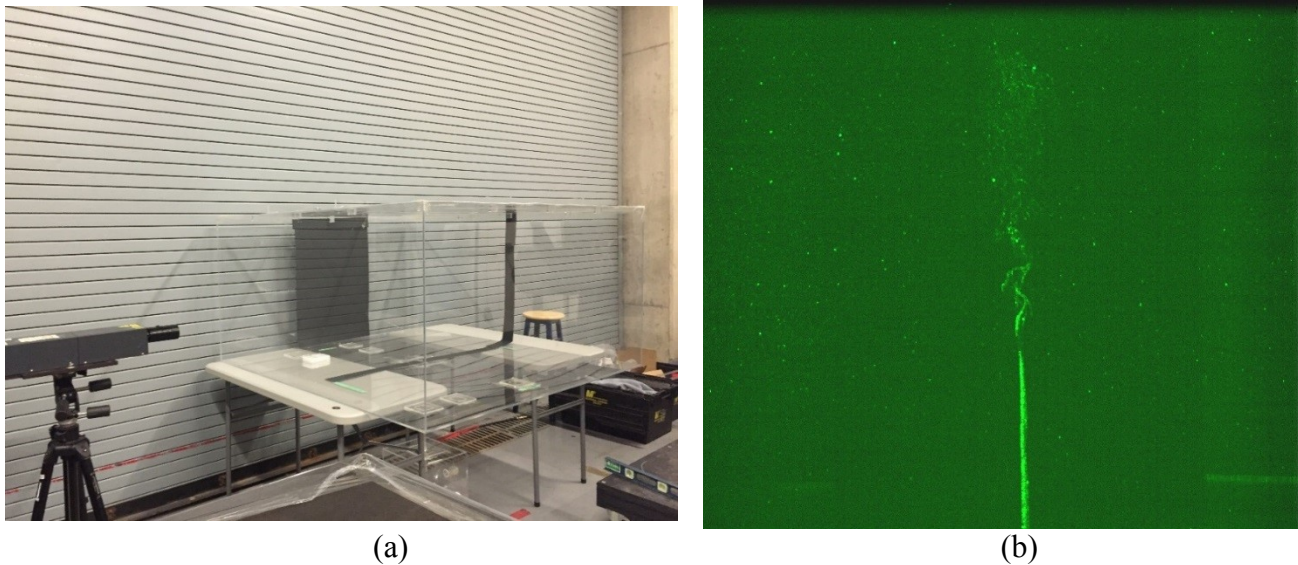
Figure 3.3 a) PIV experiment setup and b) measured helium plume graph

The commercial software ANSYS FLUENT [29] was used in this study. The geometrical model in CFD is equivalent to that of the experiment. 2nd order accuracy was used to discretize the governing Naiver – Stokes equations, A Large Eddy Simulation (LES) was applied as the turbulence model, and the PISO-SIMPLE (PIMPLE) algorithm with a time step size Δt of 4 x 10^{-7} ~ 5 x 10^{-7} for obtaining a stable solution to the discretizing equations [30,31]. A pressure outlet boundary condition was used in the ceiling and the inlet used a mass flow inlet boundary condition. The mass flow rate of helium was set as $2.0935 x 10^{-5}$ kg/s. Total release time of this study is 300 s. In this mesh model, there is in total 710,528 grid cells.

Fig. 3.4 shows the simulation results of vertical velocity at four different heights from 0-300 s. It is clear that the vertical velocity is decreased as the height is increased which matches the equation (3.8). The average vertical velocity is from 0.294 m/s to 0.214 m/s. It is shown in four different heights that the value of average vertical velocity has more fluctuation in the first 150 s. After 150 s, the flow tends to be stable. This is consistent with the study of Swain et al. [21]. In the early stage of helium release, the flow inside plume has considerable fluctuation. As a result, in the experiment, we will choose the test period from 150 s to 300 s.

In PIV experiment, we can only get the velocity results of discrete points. Fig. 3.5 shows how the average plane vertical velocity is calculated from the discrete points. Each single point was applied to one annulus, and the average vertical velocity u which is a circle was calculated based on the integral of ten annulus. Eq. (3.9) shows how the average vertical velocity is calculated.

$$u = \frac{\pi\left(r_{10}^{2} - r_{9}^{2}\right) \cdot u_{10} + \pi\left(r_{9}^{2} - r_{8}^{2}\right) + \cdots + \pi\left(r_{1}^{2}\right)}{\pi r_{10}^{2}} \tag{3.9}$$
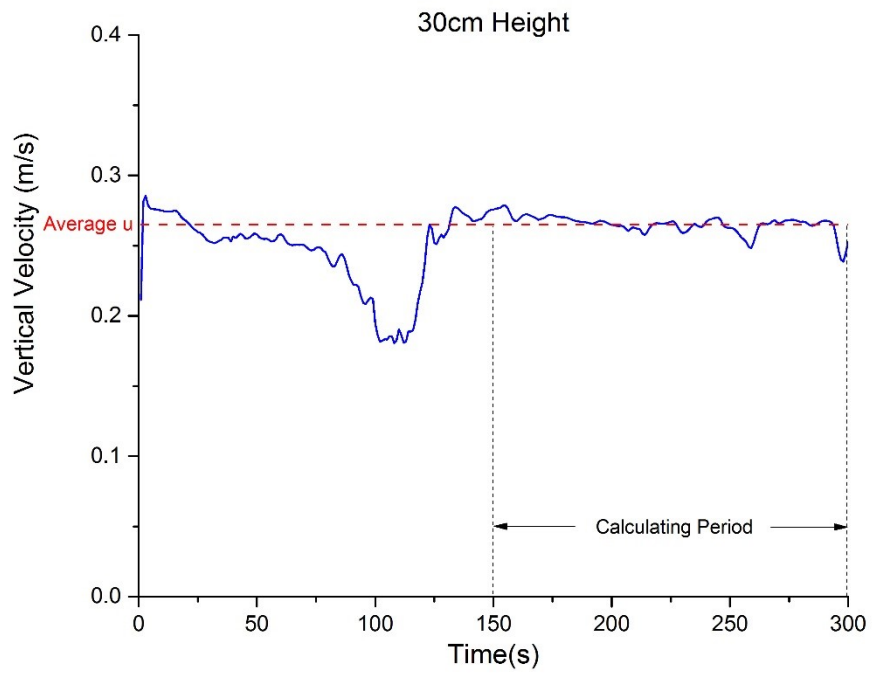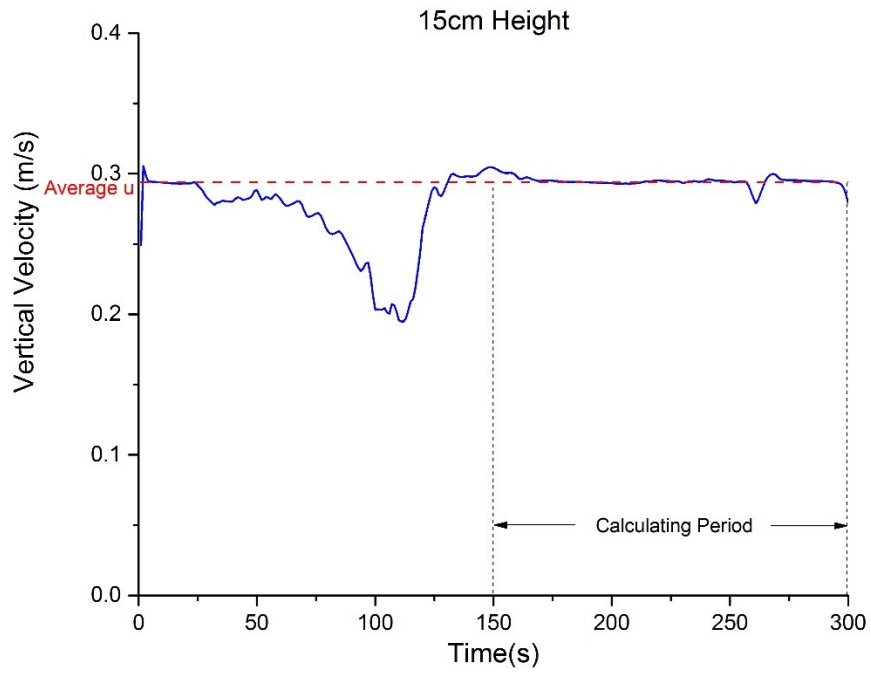
Figure 3.4 (continued)

53
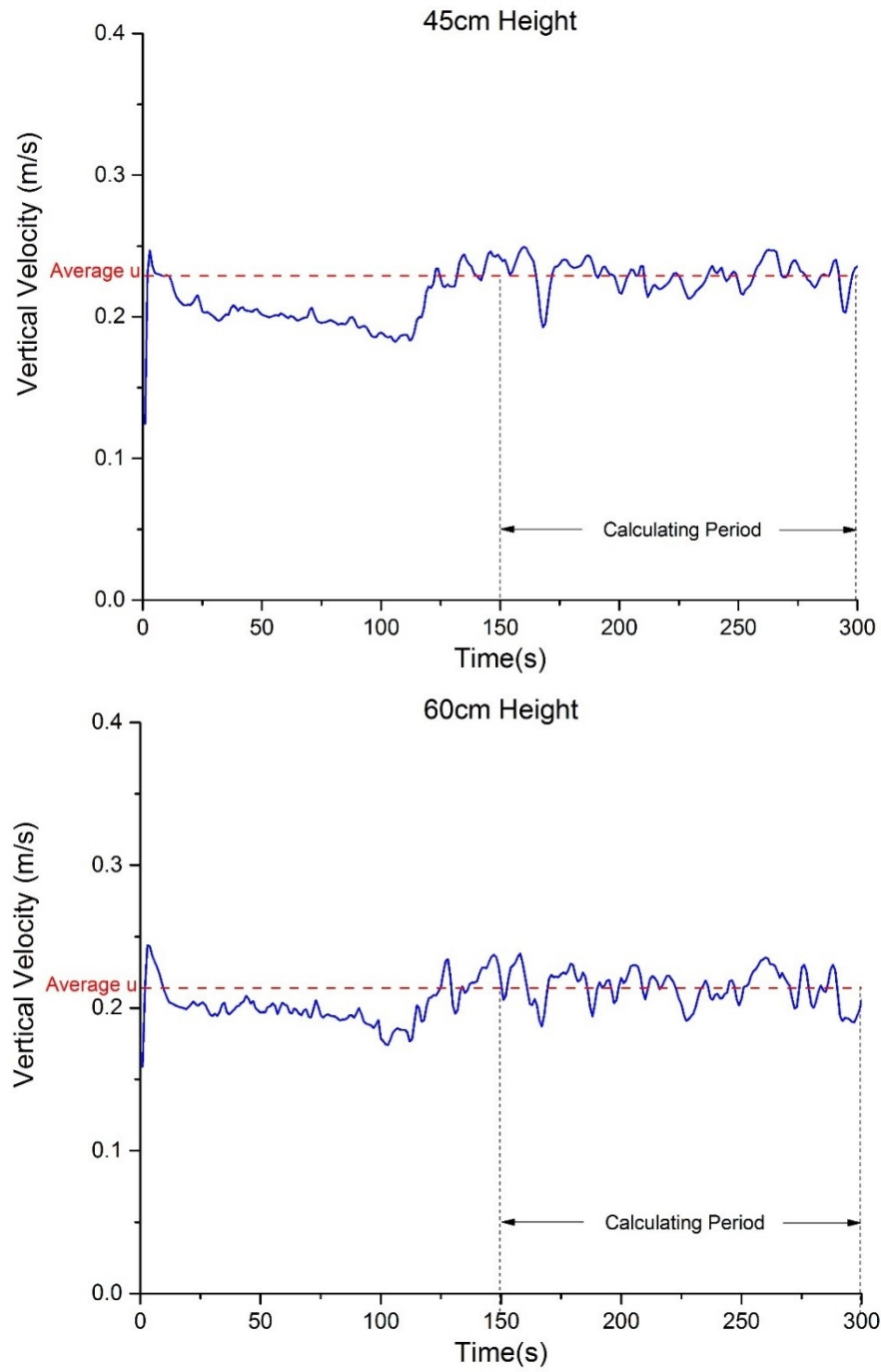
Figure 3.4 Vertical velocity of different heights in simulation from 0 ~ 300 s
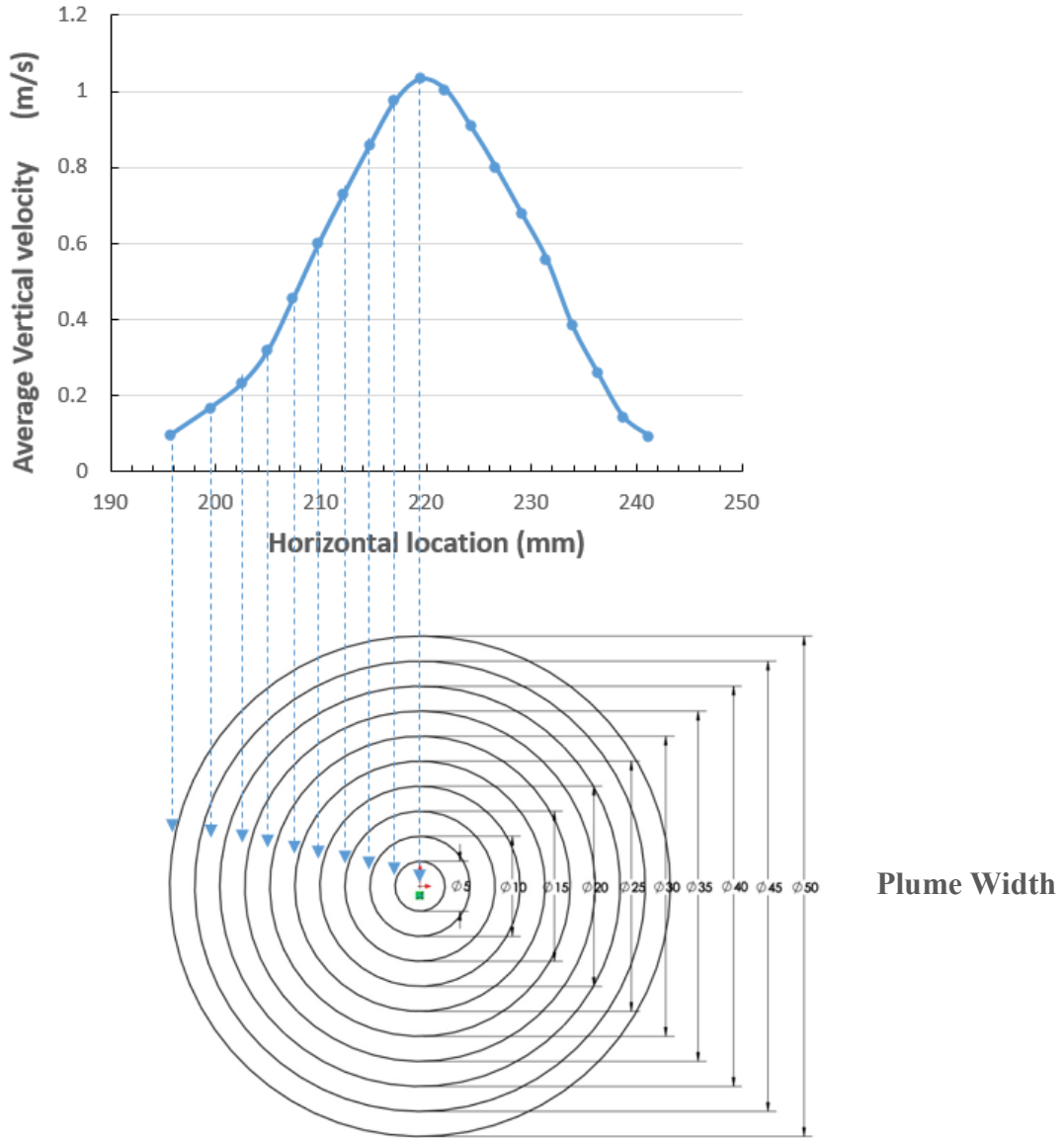
Figure 3.5 Example of calculating the average vertical velocity
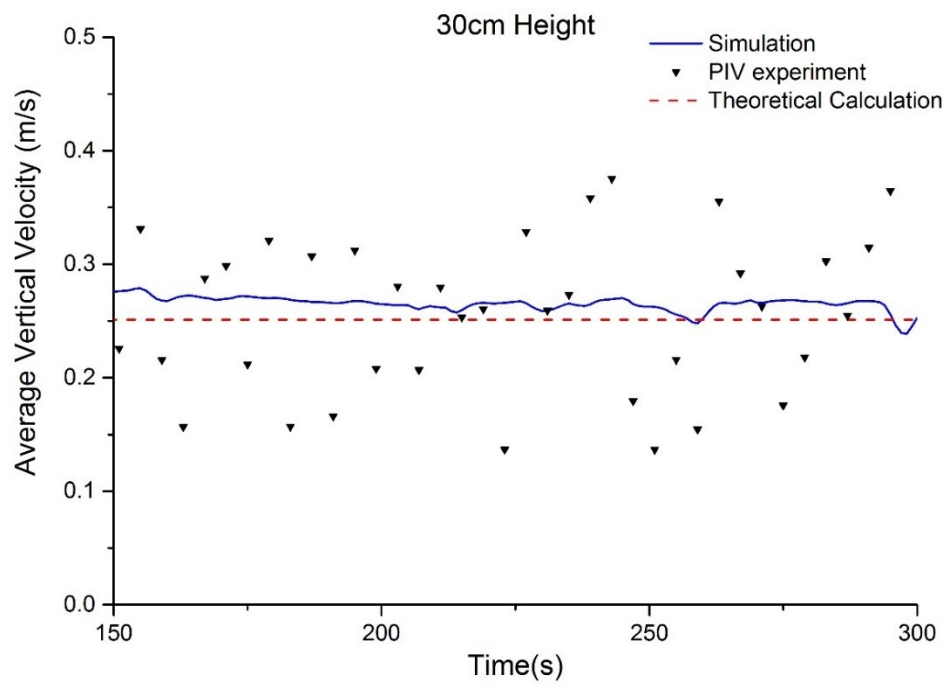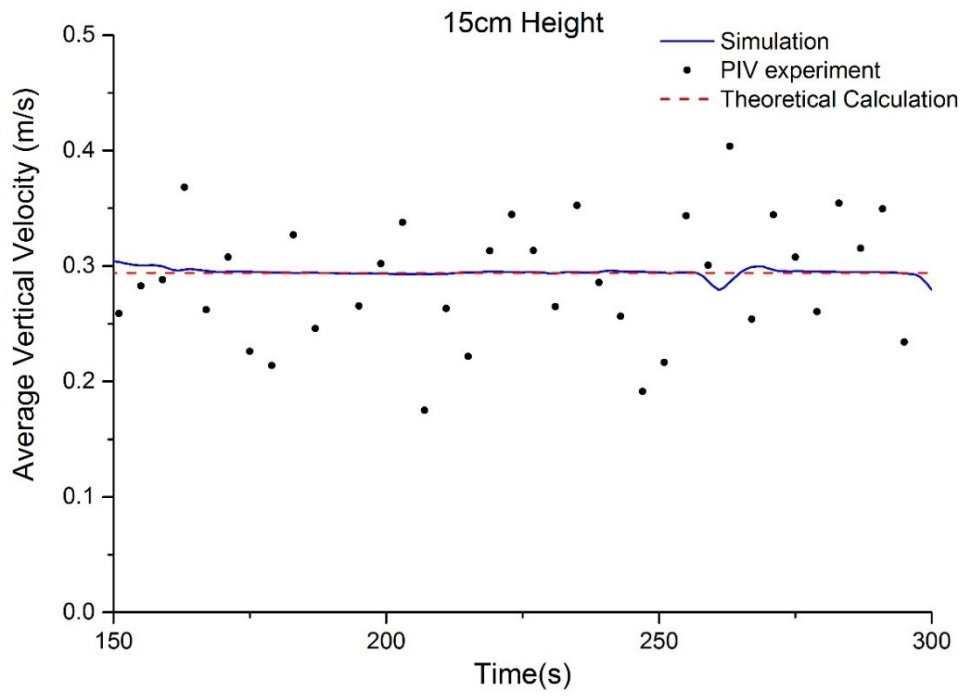
Figure 3.6 (continued)
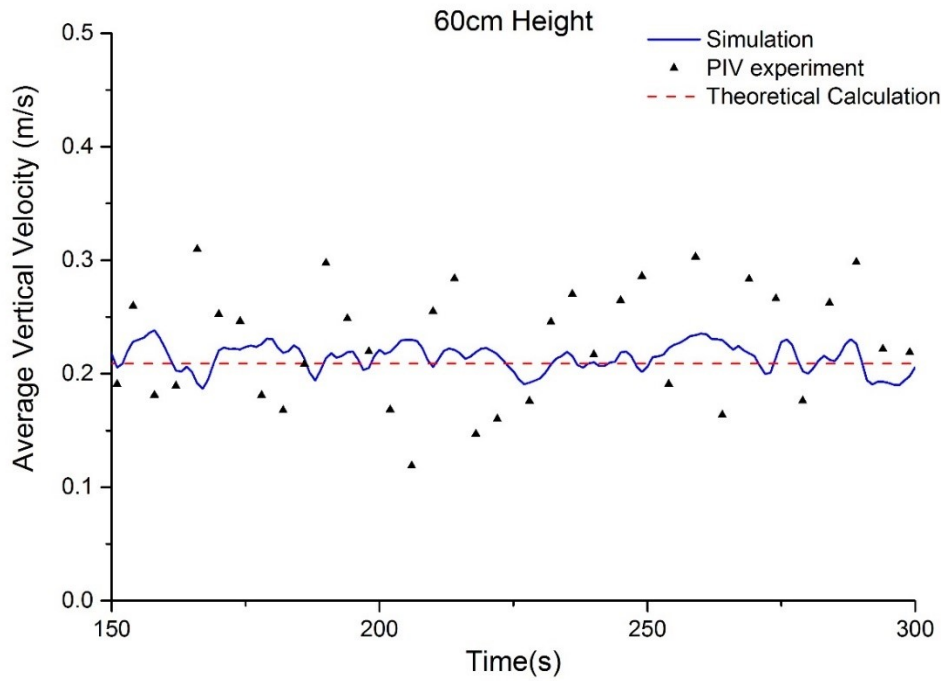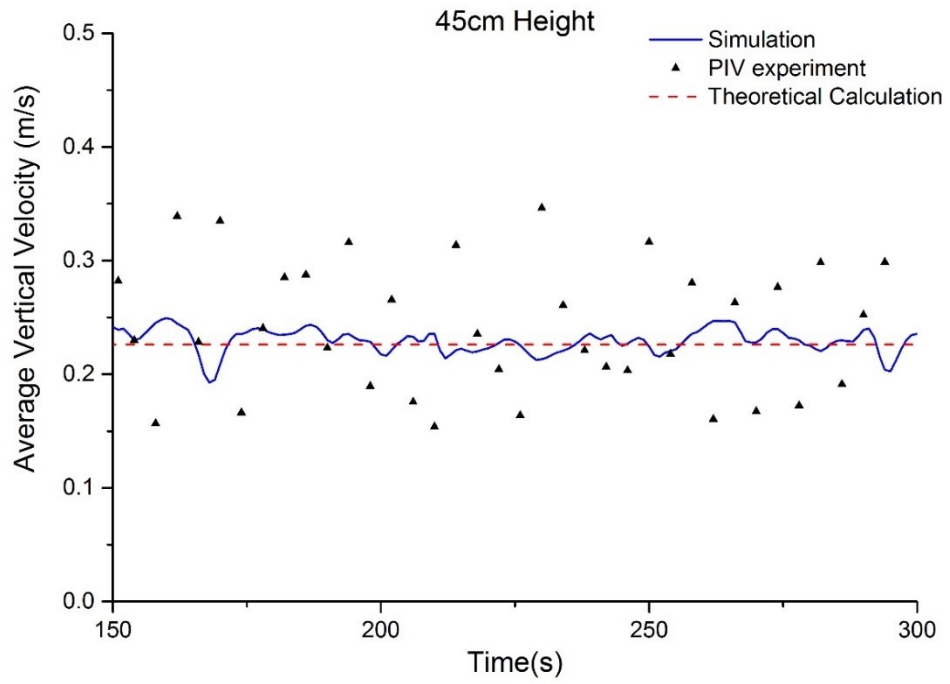
Figure 3.6 Average vertical velocity of different heights in simulation, PIV experiment and theoretical calculation.

Figure 3.6 compare the vertical velocity at different heights, in 15cm, 30cm, 45cm and 60cm, calculated from different methods (Theory, Simulation and PIV experiment). First of all, with the height increase, it is clear that the average vertical velocity is decreased. All three methods show the same decreasing tendency. All three methods show that with the height increase, the results receive more fluctuation. This is because when the height of plume increases and is close to the outlet boundary, the flow becomes more unstable. This is consistent with the previous study [22].

Table 3.1 Comparison of theoretical, simulation and experiment plume width *b(z)* in different heights

Height	Simulation (m)	Theoretical (with Eq. 3.7) (m)	Experiment 1 (m)	Experiment 2 (m)	Theoretical previous, (m)
0.00	0.02	0.02	0.02	0.02	0
0.15m	0.05	0.05	0.05	0.05	0.03
0.30m	0.08	0.08	0.08	0.08	0.05
0.45m	0.085	0.11	0.11	0.11	0.08
0.60m	0.9	0.14	0.13	0.13	0.11

Table 3.1 compares the plume width with simulation, theoretical calculation and PIV experiment in 0 m , 0.15 m, 0.30 m, 0.45 m and 0.60 m. Experiment 1 and 2 are repeat tests. The three methods well match with each other except the plume width in higher location close to the outlet boudary. With the height increase, the plume widths are enlarging. It was also found in the Eq. (3.8). There is less difference between experiment and simulation using Eq. (3.7) to calculate the plume width as compared with the previous theoretical model.

Table 3.2 Comparison of theoretical, simulation and experiment vertical velocity u in different
      height

Height	Simulation u, (m/s)		Theoretical u, use (7), (m/s)	Experiment 1 u, (m/s)		Experiment 2 u, (m/s)		Theoretical u, Previous, (m/s)
	Average	Standard deviation		Average	Standard deviation	Average	Standard deviation	
0.15m	0.294	0.003	0.294	0.298	0.085	0.299	0.089	0.373
0.30m	0.265	0.006	0.251	0.255	0.068	0.255	0.078	0.296
0.45m	0.229	0.010	0.226	0.241	0.058	0.238	0.067	0.258
0.60m	0.214	0.012	0.209	0.226	0.054	0.223	0.059	0.235

Table 3.2 compares the average vertical velocity with simulation, theoretical calculation, and PIV

experiment in 0m, 0.15m, 0.30m, 0.45m and 0.60m. Again, if we look at the average vertical

velocity, the PIV experiment shows only slight the difference with the theoretical calculation and

simulation in all heights. The standard deviation decreases with the increase of height from 0.085

to 0.054 in experiment. However, it is noticed that the standard deviation of experiment results are

larger than the simulation. Because in PIV experiment we can only measure a plane and we

calculate the average velocity from a velocity distribution in a line (19 points). On the contrary,

we can choose to calculate the average velocity of that circle surface in simulation which obviously

brings a lower standard deviation.

Meanwhile, it means that we can have smaller standard deviation or fluctuation when calculating

the average velocity, if 3D PIV measurement system is performed. We can balance the velocity

from two planes and this should bring less standard deviation.

The clear comparison of the results using the four different methods is shown in Fig. 3.7. The dots

represent the average vertical velocity and the bar shows the standard deviation. It is clear that the

new theoretical model using Eq. (3.7) brings less discrepancy with simulation and experiment for

all heights.
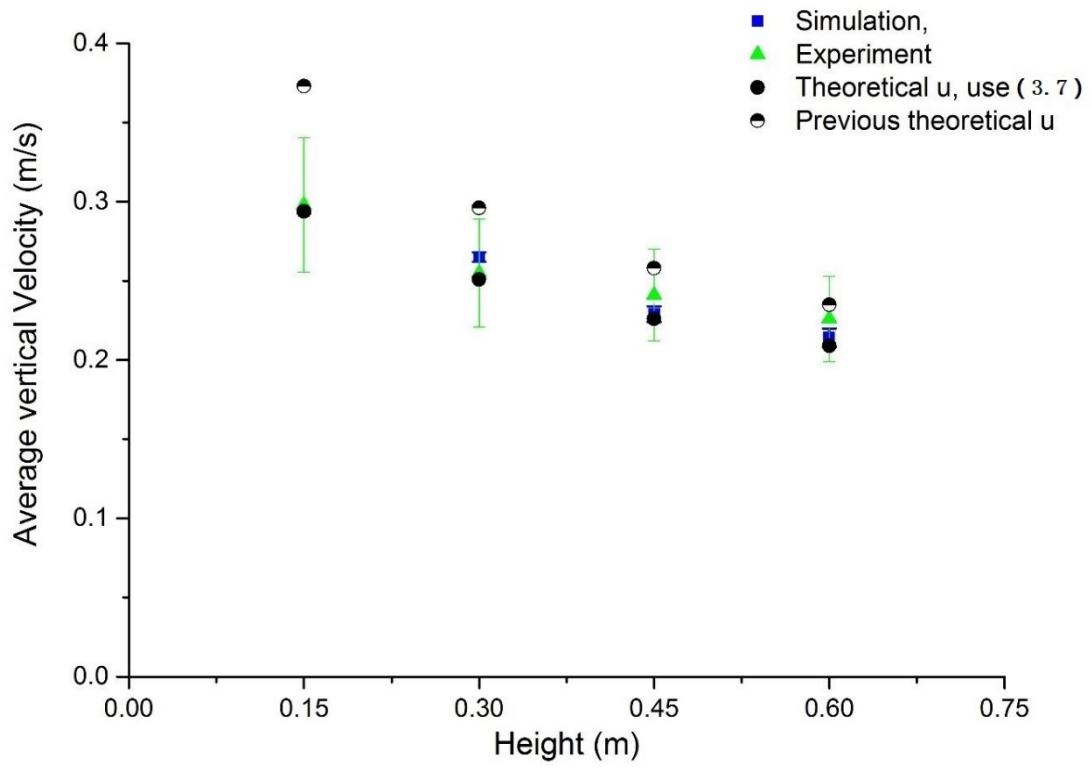
Figure 3.7 Comparison of average vertical velocity in different height in simulation, experiment, theory update and previous theory

3.4   Summary

In the previous study, most of research related to hydrogen safety focuses on the property of concentration. This section reports a new theoretical plume model which can be used in estimating the plume size and velocity. It is validated with PIV experiment and CFD simulation. The results are compared at different heights. The new theoretical model shows good accuracy among multiple heights. The present results provide a simple way to estimate the gas plume in the study of hydrogen safety and the use of helium data simulating hydrogen behavior.

4 The effect of ventilation and sunroof on hydrogen dispersion in a fuel cell vehicle

4.1 Introduction

Hydrogen is a sustainable alternative fuel that can be used to reduce foreign petroleum imports and has the added benefit of reducing environmental pollutions from combustion emission [1, 39, 40, 41, 42]. For transportation systems, hydrogen energy can be released through direct combustion process as in typical internal combustion engines using gasoline, or conversion into electrical energy in fuel cells. The latter has gained more interest due to higher efficiencies and one type of fuel cells considered in FCV applications, namely PEMFC, is very compact with high power density which can operate at low temperature facilitating system startup and providing good response to power demand required [43].

Regardless of the type of energy conversions used in hydrogen-based vehicles, or as in other hydrogen energy technology, the key challenge facing the future widespread use of hydrogen as an energy carrier is the storage safety issue that has to be addressed thoroughly before its wide usage and commercialization [44-46]. One of the main risks of using hydrogen as fuel is the problem associated with leakages and dispersion causing accidental explosion. Since hydrogen has a high buoyancy and diffusion rate in air and is often considered as extremely flammable and easily detonable gas when mixed with air over a wide range of composition (with a concentration limits of 4%-74% by volume in air), safety analysis and design of mitigation techniques against leakages and dispersion of hydrogen in different FCV scenarios have to be developed to a sufficient confidence level before social acceptance can be fully achieved.

In the literature, Computational Fluid Dynamics (CFD) is becoming a standard tool for carrying safety analysis in different real-world hydrogen release and dispersion scenarios [47-52]. A method that has been analyzed to reduce the risk of hydrogen release in an enclosure is the design of a ventilation system. A number of CFD investigations have been performed for safety analysis which suggest that for a hydrogen leak, for example from a high pressure storage, the use of a ventilation system could help to remove the flammable cloud of hydrogen reducing the risk of ignition in different scenarios, like a tunnel [20], residential garage [52], partially open space [53], fueling station [54], hydrogen laboratory [19] and FCV passenger cabin [55, 56].

In this study, the use of an active sun roof designed for FCVs is proposed to improve the mitigation technique against hydrogen release and accumulation inside a FCV compartment. This work follows closely the previous work by Salva et al. [56] who performed a safety analysis simulating the hydrogen dispersion inside the passenger cabin for different ventilation scenarios with a constant leakage rate of hydrogen. The novelty of this work is to carry out a comparative study and further explore how the effect of an active sun roof, together with the idea of designing a ventilation system, is capable of reducing the risk of hydrogen ignition inside the vehicle compartment. Using the same approach by Salva et al. [56], the leakage mass flow of hydrogen is calculated directly from the output velocity of the leak. This velocity is first modelled according to the fluid properties of hydrogen and depending only on the pressure difference between the hydrogen storage tank (350 bar) and the cabin environment. Three scenarios are considered in the present simulations, i.e., with and without the inclusion of flow rate of cabin ventilation air and the presence of the sunroof.

4.2 Numerical model and simulation details

In this study, the geometry of a general hydrogen fuel-cell vehicle (the Toyota Mirai Sedan) is used as a model for the numerical simulation. The geometry only includes the passenger seats as basic component inside the vehicle compartment. As in [56], all internal elements in the cabin that do not significantly influence the flow dynamics have been removed to simplify the computational model. The hydrogen leakage is assumed to be originated from the fuel tank stored behind the rear passengers' seats. Similar to the work by Salva et al. [56], a ventilation system is also described in the numerical model. The air ventilation system inside the cabin consists of three inlet vents on the dashboard (on the right and left side each 6 x 10 cm² and in the central area 12 x 10 cm²) and two exhaust vents in the rear pillar (on both the right and left side with an area of 0.05 m^2). The outside air is introduced into the cabin through the inlet vents and the exhaust vents allows the air flow to escape and to prevent overpressure inside the vehicle. Fig. 4.1 provides schematics of the vehicle geometry and CFD meshing from different view angles. The meshing uses the cut-cell method for the complex geometry. Unless specified, the mesh size varies from 0.004 m close to the location of hydrogen leakage to a maximum value of 0.016 m. 1,184,166 grid cells in total were contained in this computational model.

<div align="center">(a)</div>

<div align="center">(b)</div>

Front Ventilation vents

Rear exhaust vents

Leakage

<div align="center">(c)</div>
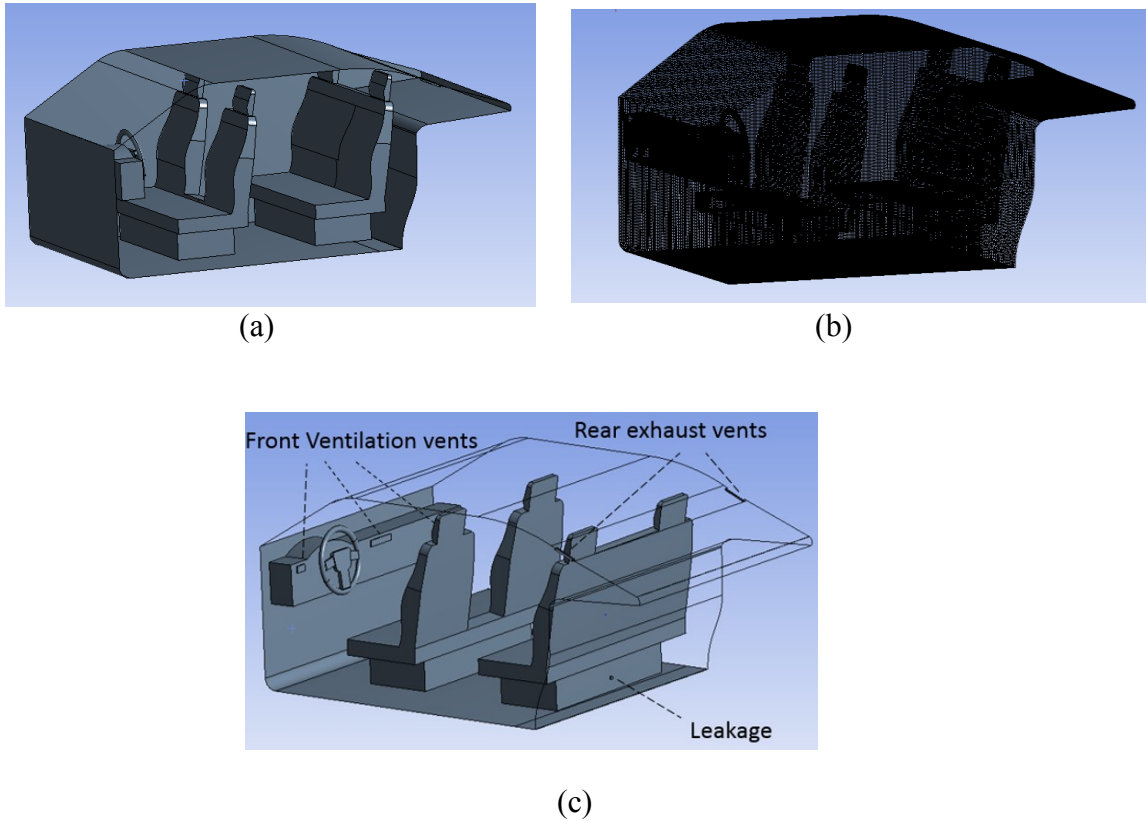
Figure 4.1 a), b) Geometry; and c) CFD mesh of the fuel cell vehicle model

The commercial software ANSYS-FLUENT [29] is used in this study for the numerical simulation. All the scenarios are performed in transient state simulation. The computation uses a finite volume scheme with 2nd order accuracy to discretize the governing Navier-Stokes equations. A Large Eddy Simulation (LES) was applied as the turbulence model, and the PISO-SIMPLE (PIMPLE) algorithm with a time step size Δt of 0.025 s to obtain a stable solution to the discretized equations [29-31]. All the numerical simulations were performed using the computer cluster available at the High Performance Computing Virtual Laboratory (HPCVL) managed by Compute Canada [32].

For the computational default setting, the initial temperature of released hydrogen and air temperature in the cabin were set equal to 294 K and initial pressure to 101 kPa. The ventilation

vents use the velocity inlet boundary condition of 2 m/s. A pressure outlet boundary condition is employed for the exhaust vents. The hydrogen leakage is modelled using a mass flow inlet boundary condition. Following the approach by Salva et al. [56], the mass leakage rate is determined according to the hydrogen storage pressure in the tank. The release velocity V_s (m/s) is first obtained using Eq. (4.1) for isentropic flow:

$$V_s = \sqrt{\frac{\gamma P}{\rho}} \left(1 + \frac{\gamma - 1}{2}\right)^{-\frac{1}{2}} \qquad (4.1)$$

where γ is the adiabatic coefficient P is the pressure of hydrogen storage. Using the continuity equation, the mass flow rate is given as:

$$\dot{m} = \rho \cdot A \cdot V_s \qquad (4.2)$$

In this study, a typical hydrogen storage pressure of 350 bar and a leakage area of $A = 3.14 \times 10^{-6}$ m^2 are used. Solving Eqs. (4.1) and (4.2), the outlet velocity and the mass flow rate are determined to be $V_s = 1264$ m/s and $\dot{m} = 3.2 \times 10^{-4}$ kg/s. As noted in [56], this approach is a modelling simplification to the real hydrogen release phenomenon since the flow dynamics of an actual supersonic compressible flow with shocks is not considered in this leakage model. The results are nevertheless representative of leakage scenarios within the vehicle cabin away from the origin of the hydrogen leakage and should be sufficient for the present comparative study.

4.3 Results and discussion

Three cases are simulated for the present comparative study. Simulation A is the base case without any ventilation and sunroof. Simulation B is similar to the cases investigated by Salva et al. [56] with both the front and rear vents activated. Simulation C extends the Simulation B scenario by including an automobile sunroof. In all simulation cases, the hydrogen leak rate and all other factors are kept the same. The leakage time is approximately 100 s by considering the volume of fuel pipe.
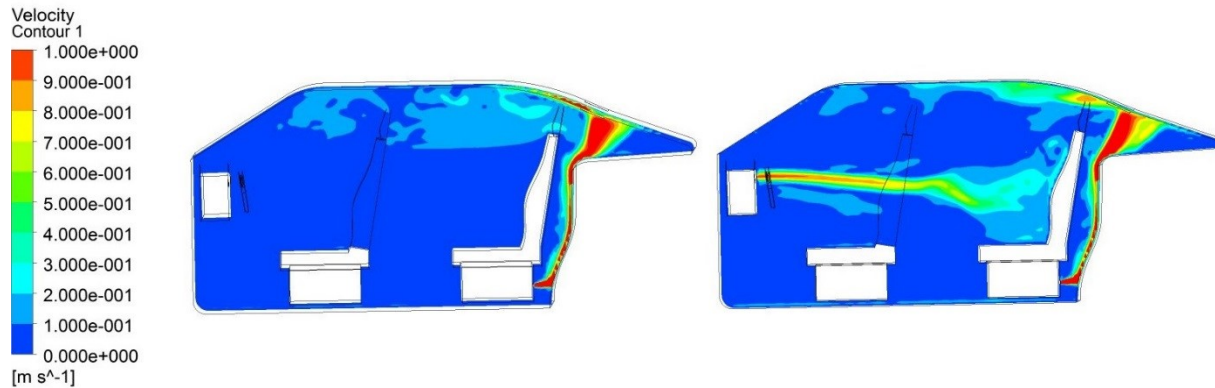
Figure 4.2 Velocity contours in longitudinal plane at 100 s for Simulation A (left); and Simulation B (right).

From Fig. 4.2, it is clear that the flow dynamics is totally different between Simulation A and simulation B. There is nearly no longitudinal flow in Simulation A. Nonetheless, majority of hydrogen is accumulated at the top in both cases due to its strong buoyancy and dispersion rate. Figure 4.3 shows the hydrogen concentration distribution for Simulation B where the front and rear vents are modelled. It indicates well that the hydrogen concentration increases when the vertical position gets higher. At a vertical height of 1.4 m, a large hydrogen concentration at 10%

is accumulated. At this level, it comes the ignition risk since the concentration is within the flammability limit. The hydrogen concentration is below 4% (or outside the flammability limit) only at the height below 1.1 m.
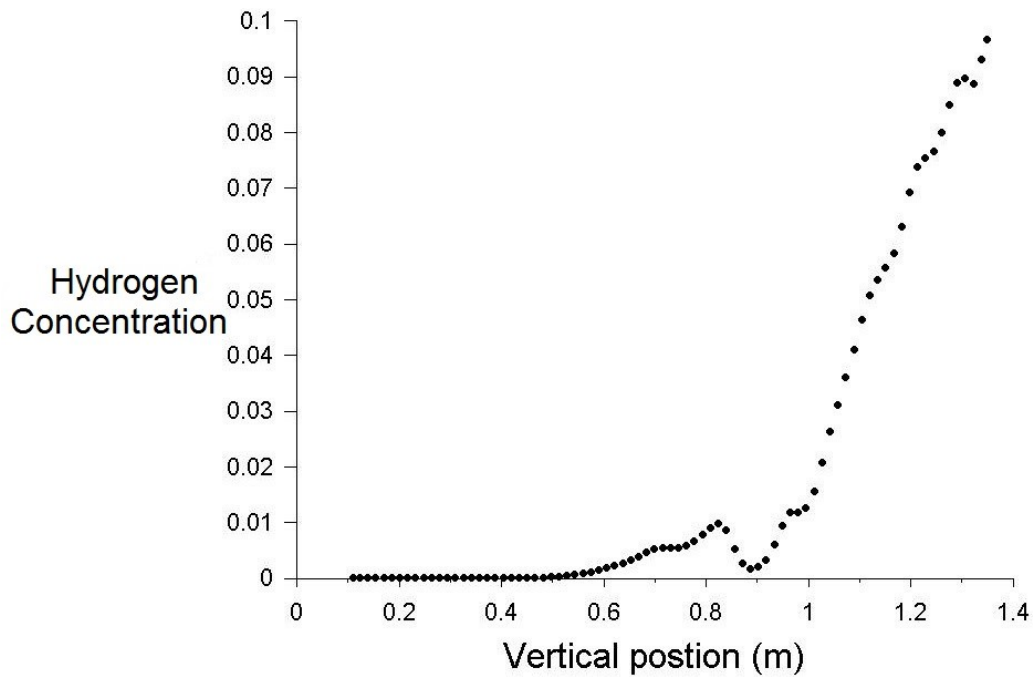
Figure 4.3 Hydrogen concentration in vertical position at 100 s for Simulation B

Inspired by the results given in Figs. 4.2 and 4.3, a simulation scenario with a sunroof (100x40 cm) is designed in this study (Simulation C). The position of the sunroof is shown in Fig. 4.4a. It is assumed that the sunroof has an active control unit which is connected with a hydrogen sensor in the car ceiling. These communicate with each other through a Controller Area Network (CAN). It can be programmed such that the sunroof will open immediately when there is a hydrogen leakage in this vehicle or accumulation above the allowable threshold, see Fig. 4.4b. In the simulation, the boundary condition for this sunroof was set as pressure-out. It is believed that the

68

sunroof design could play an extra ventilation in the case of emergency of hydrogen leakage and unexpected accumulation.
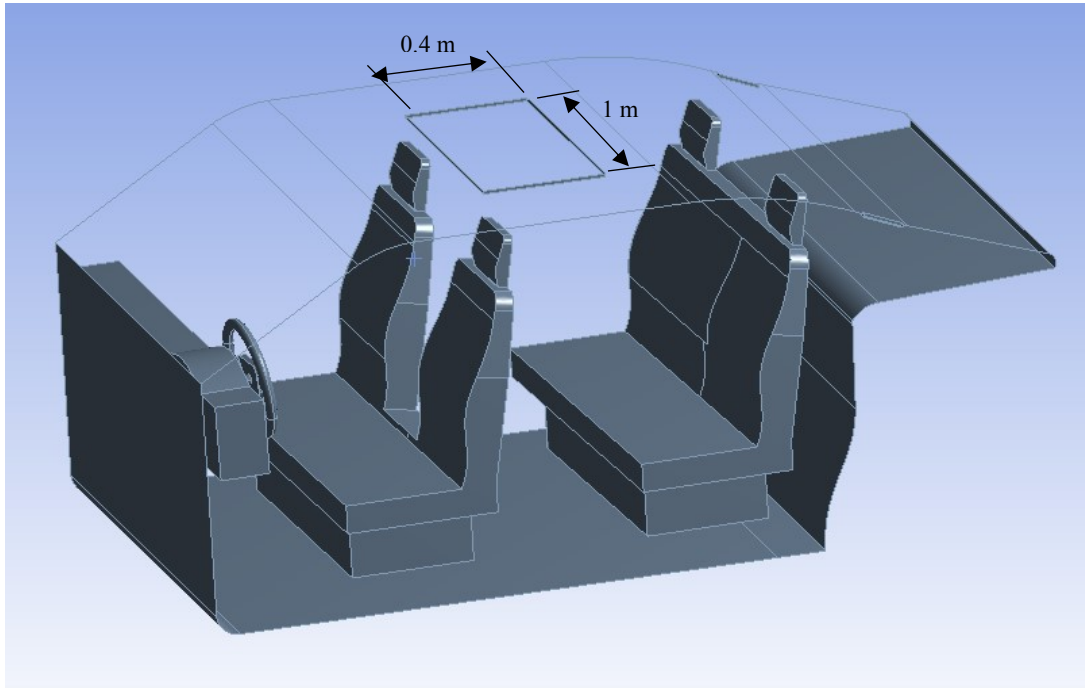
(a)
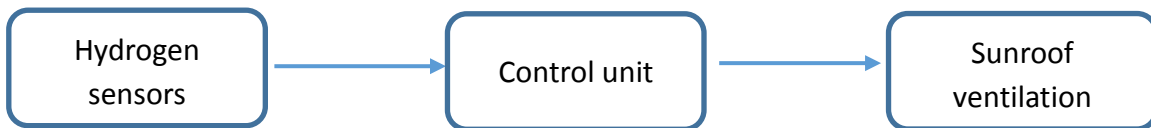
(b)

Figure 4.4 a) Position of the sunroof ; and b) layout of an active sunroof system in a fuel-cell vehicle

Fig. 4.5 shows the hydrogen concentration zones with danger of inflammation, i.e., the location where the hydrogen concentration is found within 4% to 75%. It gives the value of the inflammable volume directly. Simulation A (no vents) has the largest value of inflammable volume among the

three simulation cases. Without the ventilation system, hydrogen disperses and accumulates covering all the car ceiling. Simulation B (with vents) has less inflammable volume than simulation A. Nevertheless, there is still considerable amount of hydrogen inside the vehicle representing an ignition risk. It is clear that there is the lowest hydrogen concentration accumulation in Simulation C (with sunroof). The average concentration inside the vehicle is 2.3% for Simulation C, which is under 4%. On the contrary, hydrogen concentration accumulated in the cabin for both Simulations A and B, 25.9% and 11.2%, respectively, are much larger than 4% within the flammable limit of hydrogen. The hydrogen concentration level found for Simulation A, 25.9%, even exceeds the detonability limit of hydrogen which is 18.3%. Therefore, the present results show that Simulation C (with sunroof) has the least risk of fire and explosion. The use of the sunroof prevents the hydrogen gas to be trapped at the vehicle ceiling and also the momentum of impingement of the hydrogen flow from the release point to the ceiling is reduced, hence diminishing the mixing between the hydrogen and air.

Central plane was chosen to show the vertical distribution of hydrogen concentration, given in Fig. 4.6. Simulation A has a partially steady flow inside the vehicle. The mixture gas inside the cabin is divided into serial layers. In all the cases, the high concentration level of hydrogen is found after the rear seat where the storage tank or leakage is located. Both Simulations B and C show a more complex flow in the longitude view where the hydrogen concentration distribution is less uniform. Closer to the vent and sunroof, the hydrogen concentration is greatly reduced. Lateral distributions of hydrogen concentration are shown in Fig 4.7. All three graphs show essentially a symmetry characteristics of hydrogen distribution. The results are consistent with those shown in Fig. 4.5. Again, Simulation A has the largest concentration and Simulation C has the lowest concentration of hydrogen. Meanwhile, the boundary of sunroof can be seen from Fig. 4.7 (c). Around where,

70

hydrogen concentration decreases compared with other location which has the same vertical height, see Fig. 4.8.
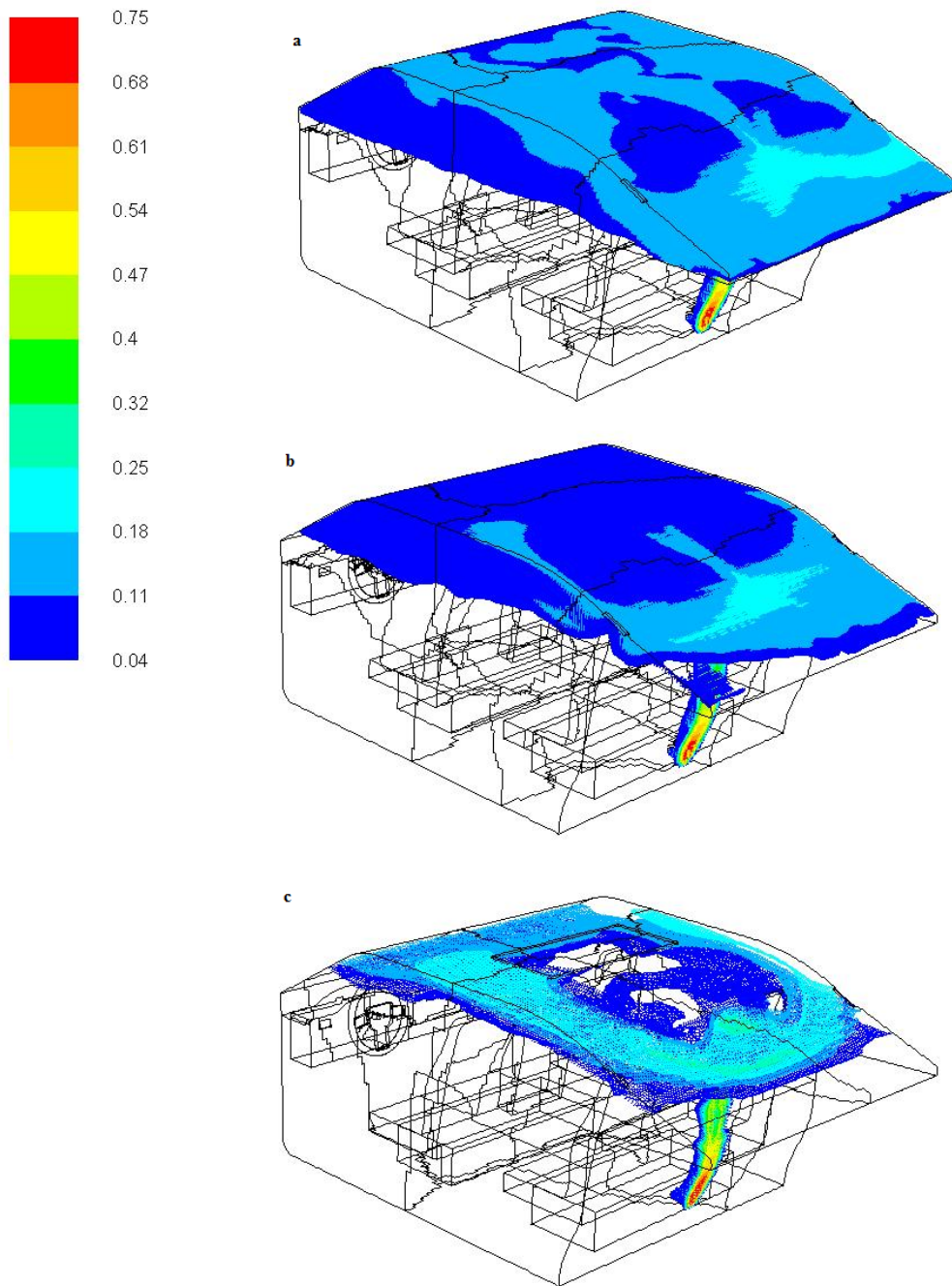

Figure 4.5 Hydrogen concentration contours at 100 s showing zone of ignition risk in a) Simulation A; b) Simulation B; and c) Simulation C
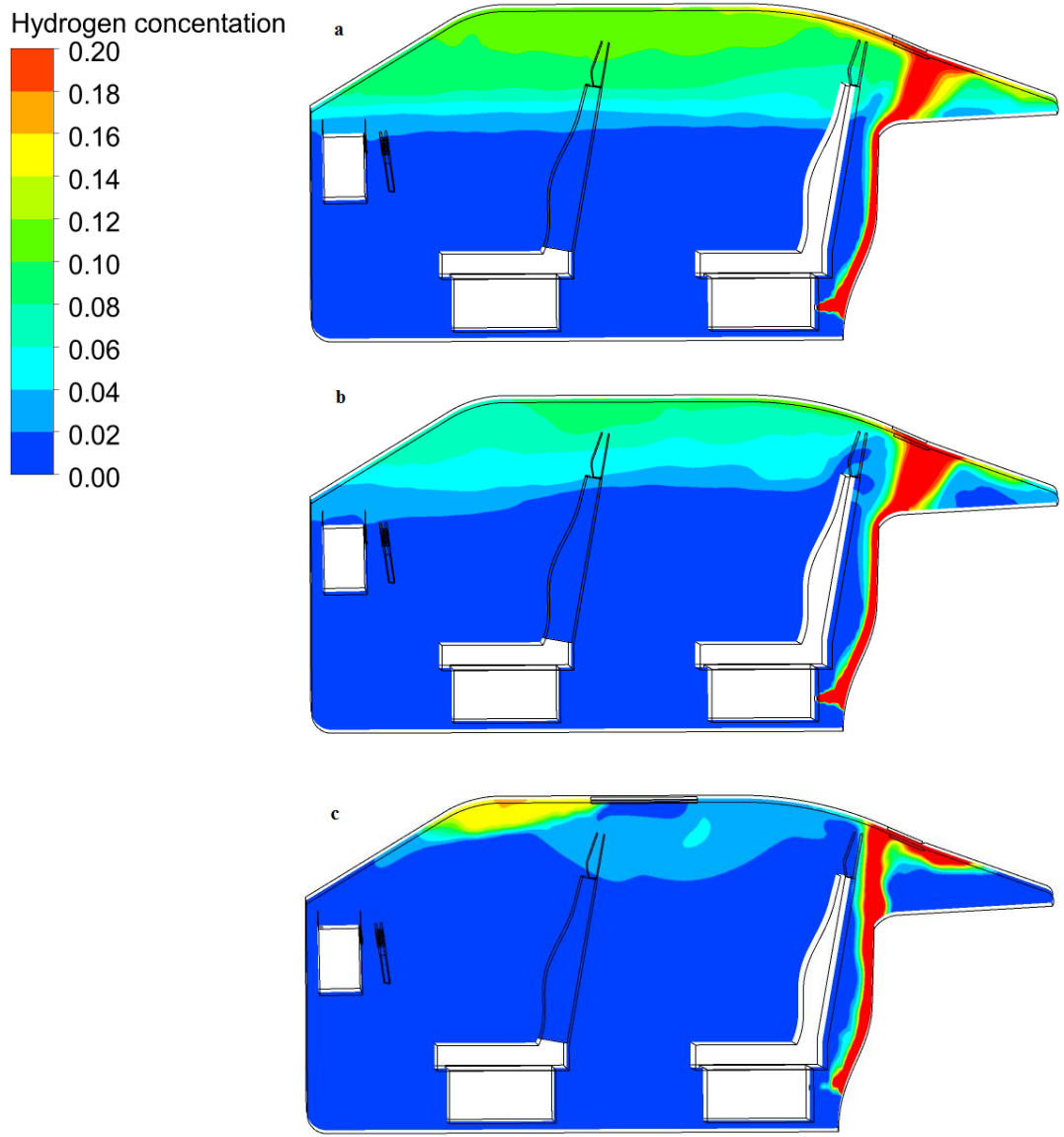
Figure 4.6 Hydrogen concentration in longitudinal plane at 100 s of a) Simulation A; b) Simulation
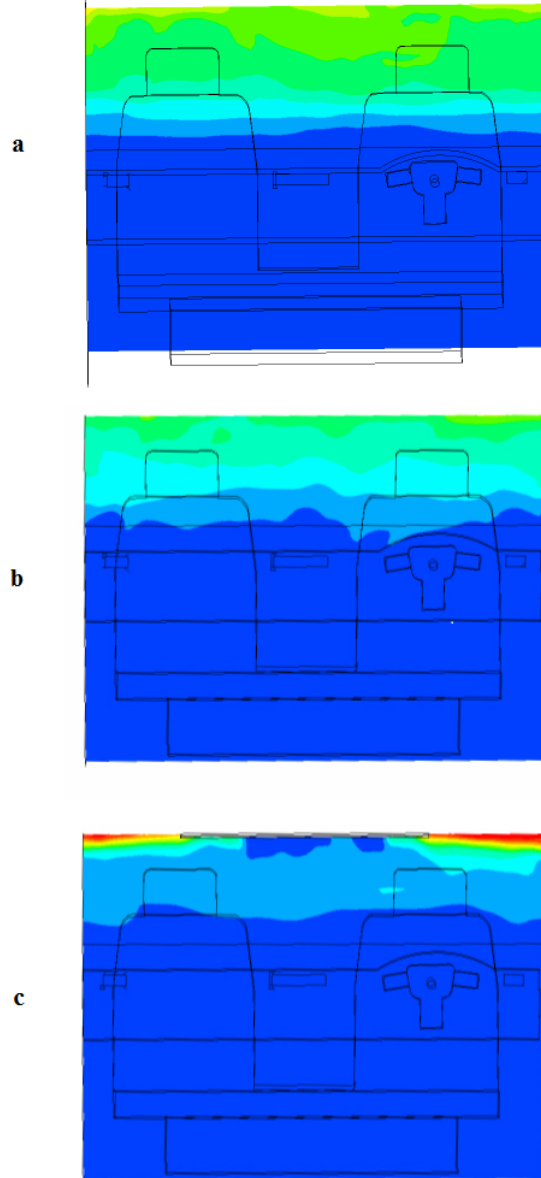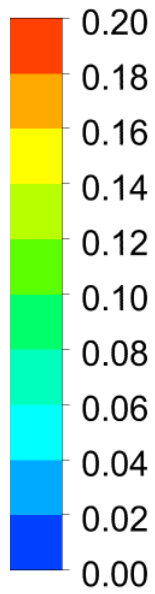
B; and c) Simulation C

Figure 4.7 Hydrogen concentration in lateral plane at 100 s of a) Simulation A; b) Simulation B; and c) Simulation C
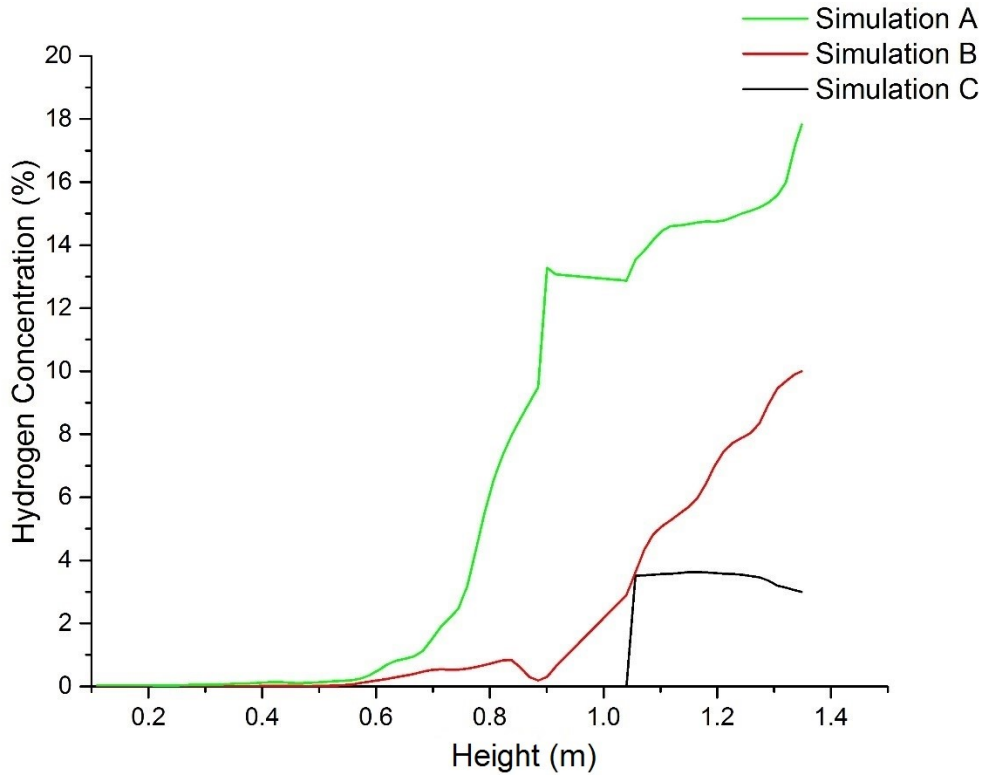
Figure 4.8 Hydrogen concentration in vertical height at 100 s for all simulation cases.

Figure 4.8 is plotted at the center point of this vehicle showing the detailed vertical concentration distribution. There is a noticeable decrease of hydrogen concentration for Simulation C after the height of 1.1 m due to the effect of sunroof. For Simulation B with ventilation but not the sunroof, the hydrogen concentration still increases continuously at 1.1 m reaching a peak concentration of 10% at 1.4 m, but with a smaller rate as compared to the Simulation A. Generally speaking, the hydrogen concentration increases and accumulates at higher height in all three simulations. As a result, the ventilation and exhaust vents can help reduce the risk of hydrogen accumulation when the upper layer flow is increased, which could be an important design guide for the ventilation system of FCV.

4.4   Summary

In this work, CFD method is used to simulate a hydrogen leakage inside a FCV cabin. Following the previous study [56], hydrogen leakage rate was calculated from specific storage pressure. Three scenarios, i.e., no vents, vents and sun roof, were simulated to compare their different effects on the hydrogen concentration distribution. The present results indicate that good ventilation system is crucial to reduce the hydrogen concentration within the FCV cabin in a leakage case. Sunroof can further decrease the risk of hydrogen ignition to a great extent, preventing hydrogen gas to be trapped at the ceiling and reducing the momentum of impingement which can enhance mixing. For the hydrogen sensor placement, it should be set close to the car ceiling due to the high buoyancy of hydrogen. Present results are encouraging and should be validated in different leakage locations. Future work should focus on the effect of vehicle speed on the hydrogen leakage for FCV using dynamic mesh. Overall, those data could be used as a reference in the future FCV design and demonstrate the feasibility of using CFD simulation to predict the concentration of hydrogen.

5 Conclusion and future work

5.1 Conclusion

This thesis studied three correlations for the similarity between hydrogen and helium. The accuracy of these correlations at different stages of release and location is assessed using the validated CFD model. The results can help to verify numerical approach in the study of hydrogen safety and the use of helium data for hydrogen dispersion analysis.

An updated theoretical helium plume model is also proposed, which can be used in estimating the plume size and velocity. The new model was validated in different plume heights using CFD method and PIV experiment.

A case study of a hydrogen leakage inside a FCV cabin is simulated with the CFD method. This study compares the different effects on the hydrogen concentration distribution in three scenarios (no vents, vents and sun roof). The results find that the ventilation systems are important to reduce the hydrogen concentration within the FCV cabin in a leakage case. Sunroof can further decrease the hydrogen concentration to a large extent. Those data could be used as a reference in the future FCV design and demonstrate the feasibility of using CFD simulation to predict the concentration of hydrogen.

5.2 Future work

In the PIV experiment which is used to validate the new theoretical helium plume model for different plume heights, relative large standard deviation are obtained in the results. More experiments are needed in the future to get the more accurate velocity values by using 3D Time –

Resolved Particle Image Velocimetry (TR-PIV). Such measurements received from two cameras will allow a lower standard deviation by obtaining average velocity in planes.

For the simulation of hydrogen leakage in FCV, the numerical vehicle model is static. A dynamic mesh is expected in the future to simulate the ventilation effect in different vehicle speeds, which is closer to the reality.

Meanwhile, all the experiments done in this thesis are sub-scale experiments in an enclosure. In the future, full size experiments or complex geometries [57] are desirable for more in-depth analysis.

6   References

[1]   Züttel, A. (2010) Hydrogen: The future energy carrier. *Phil. Trans. Roy. Soc. A* 368: 3329-3342.

[2]   U.S. Department of Energy (2004) *Module I - Permitting Stationary Fuel Cell Installations*. Version 1.0, PNNL-14518 Released 1/12/2004.

[3]   GM Electrovan.(1966). *Hydrogen Cars Now*. Avaliable from: ⟨http://www.hydrogencarsnow.com/index.php/gm-electrovan/⟩, 2011.

[4]   Kazempoor, P., Dorer, V., & Ommi, F. (2009) Evaluation of hydrogen and methane-fuelled solid oxide fuel cell systems for residential applications: System design alternative and parameter study. *Int. J. Hydrogen Energy* 34: 8630-8644.

[5]   Shah, A., Mohan, V., Sheffield, J. W., & Martin, K. B. (2011) Solar powered residential hydrogen fueling station. *Int. J. Hydrogen Energy* 36: 13132-13137.

[6]   Netinform. *Hydrogen Filling Stations Worldwide.* Available from: http://www.netinform.net /H2/H2Stations/Default.aspx⟩, 2014.

[7]   CFCP. *A California Road Map Bringing Hydrogen Fuel Cell Electric Vehicles to the Golden State*. Available from: ⟨http://www.cafcp.org/roadmap⟩, 2012.

[8]   Fuel Cells 2000. *U.S. Hydrogen Fueling Stations.* Available from: ⟨http://www.fuelcells.org /uploads/h2fuelingstations-US4.pdf⟩, 2013.

[9]   Matthey, J. *27 New Hydrogen Stations Worldwide in 2012*. Available from: ⟨http://www.fuelcelltoday.com/news-archive/2013/march/27-new-hydrogen-stations-worldwide-in-2012⟩, 2013.

[10]   Hashimoto, M. *Status of National H_2 and Fuel Cell Programmes in Japan*. Available from:

⟨http://www.iphe.net/partners/japan.html⟩, 2012.

[11] Kim, J. *Recent Achievements in Hydrogen and Fuel Cells in Korea*. Available from: ⟨http://hydrogenius.kyushu-u.ac.jp/cie/event/ihdf2013/pdf/2-3kim.pdf⟩, 2013.

[12] Lipman, T. *An Overview of Hydrogen Production and Storage Systems with Renewable Hydrogen Case Studies*. Conducted under US DOE Grant: DE-FC3608GO18111A000, Office of Energy Efficiency and Renewable Energy Fuel Cell Technologies Program, 2011.

[13] ANSI/ASHRAE. *Standard 62.2 Ventilation for Acceptable Indoor Air Quality*, 2013.

[14] Dodds, P., Staffell, I., Hawkes, A.D., Li, F., Grünewald, P., McDowall, W., & Ekins, P. (2015) Hydrogen and fuel cell technologies for heating: A review. *Int. J. Hydrogen Energy* 40(5): 2065-2083.

[15] Ng, H.D., & Lee, J.H.S. (2008) Comments on explosion problems for hydrogen safety. *J. Loss Prev. Proc. Ind.* 21: 136-146.

[16] U.S. Department of Energy Hydrogen Safety Fact Sheet Series.

[17] Prasad, K., Pitts, W., & Yang, J. (2011) A numerical study of the release and dispersion of a buoyant gas in partially confined spaces. *Int. J. Hydrogen Energy* 36: 5200-5210.

[18] LaChance, J.L., Tchouvelev, A., & Ohi, J. (2009) Risk-informed process and tools for permitting hydrogen fueling stations. *Int. J. Hydrogen Energy* 34: 5855-5861.

[19] Heitsch, M., Baraldi, D., & Moretto, P. (2010) Numerical analysis of accidental hydrogen release in a laboratory. *Int. J. Hydrogen Energy* 35(9): 4409-4419.

[20] Middha, P., & Hansen, O.R. (2009) CFD simulation study to investigate the risk from hydrogen vehicles in tunnels. *Int. J. Hydrogen Energy* 34(14):5875-5886.

[21] Swain, M. R., Filoso, P., Grilliot, E. S., & Swain, M. N. (2003) Hydrogen leakage into simple geometric enclosures. *Int. J. Hydrogen Energy* 28:229-248.

[22] Choi, J., Hur, N., Kang, S., Lee, E.D., & Lee, K. B. (2013) A CFD simulation of hydrogen dispersion for the hydrogen leakage from a fuel cell vehicle in an underground parking garage. *Int. J. Hydrogen Energy* 38(9):8084-8091.

[23] Swain, M.R., Grilliot, E.S., & Swain, M.N. (2002) The application of a hydrogen risk assessment method to vented spaces. In: *Advances in Hydrogen Energy*. Springer, NY, pp. 163-173.

[24] Swain, M.R., Grilliot, E.S., & Swain, M.N. (1999) Experimental verification of a hydrogen risk assessment method. *Chem. Health Safety* 6(3):28-32.

[25] Karlsson, B., & Quintiere, J. (1999) *Enclosure Fire Dynamics*. CRC Press, Florida.

[26] Kokgil, E. (2015) *Using Helium as Hydrogen Surrogate for Safety Analysis Related to Hydrogen Leaks from Residential Fuel Cell Systems*. Master thesis, Concordia University, Montreal, Canada.

[27] Wang, L., & Zhao, G. (2013) Numerical study on smoke movement driven by pure helium in atria. *Fire Safety J.* 61:45-53.

[28] Zhao, G., & Wang, L. (2014) Using helium smoke as a surrogate of fire smoke for the study of atrium smoke filling. *J. Fire Sci.* 32(5):431-447.

[29] *ANSYS FLUENT 14.5 User's Guide.* ANSYS. 2009.

[30] Barton, I.E. (1998) Comparison of SIMPLE- and PISO-type algorithms for transient flows. *Int. J. Numer. Meth. Fluids* 26:459-483.

[31] Ferziger, J., & Peric, M. (1999) *Computational Methods for Fluid Dynamics*. 2nd ed. Springer-Verlag, Berlin.

[32] High Performance Computing Virtual Laboratory. (2015) Retrieved from
http://www.hpcvl.org/

[33] Patankar, S.V. (1980) *Numerical Heat Transfer and Fluid Flow*. Hemisphere, Washington DC.

[34] Wipke, K., Welch, C., Thomas, H., Sprik, Gronich, S., & Garbak, J. (2009) *Controlled Hydrogen Fleet and Infrastructure Demonstration and Validation Project*. National Renewable Energy Laboratory, NREL/JA-560-40921.

[35] EG & G Technical Service Inc. (2004) *Fuel Cell Handbook* (Seventh Edition). West Virginia, U.S. Department of Energy Office of Fossil Energy.

[36] Cariteau, B., Brinster, J., Studer, E., Tkatschenko, I., & Joncquet, G. (2009) Experimental results on the dispersion of bouyant gas in a full scale garage from a complex source. *Int. J. Hydrogen Energy* 36(3):2489-2496.

[37] He, J., Kokgil, E., Wang, L., & Ng, H.D. (2016) Assessment of similarity models using helium for prediction of hydrogen dispersion in an enclosure. *Int. J. Hydrogen Energy* 41(34): 15388-15398.

[38] Pitts, M.W., Yang, J.C., Matthew, B., & Joyce, A. (2012) Dispersion and burning behavior of hydrogen released in a full-scale residential garage in the presence and absence of conventional automobiles. *Int. J. Hydrogen Energy* 37(22):17457-17469.

[39] Balat, M. (2008) Potential importance of hydrogen as a future solution to environmental and transportation problems. *Int. J. Hydrogen Energy* 33(15):4013-4029.

[40] Cipriani, G., di Dio, V., Genduso, F., La Cascia, D., Liga, R., Miceli, R., & Galluzzo, G.R. (2014) Perspective on hydrogen energy carrier and its automotive applications. *Int. J. Hydrogen Energy* 39(16):8482-8494.

[41] Jacobson, M.Z., Colella, W.G., & Golden, D.M. (2005) Cleaning the air and improving health with hydrogen fuel-cell vehicles. *Science* 308(5730):1901-1905.

[42] Schlapbach, L. (2009) Technology: Hydrogen-fuelled vehicles. *Nature* 460:809-811.

[43] Wieser, C. (2004) Novel polymer electrolyte membranes for automotive applications - Requirements and benefits. *Fuel Cells* 4(4):245-250.

[44] DeLuchi, M.A. (1989) Hydrogen vehicles: an evaluation of fuel storage, performance, safety, environmental impacts, and cost. *Int. J. Hydrogen Energy* 14(2):81-130.

[45] Najjar, Y.S.H. (2013) Hydrogen safety: The road toward green technology. *Int. J. Hydrogen Energy* 38(25):10716-10728.

[46] Reider, R., & Edeskuty, F.J. (1979) Hydrogen safety problems. *Int. J. Hydrogen Energy* 4(1):41-45.

[47] Venetsanos, A.G., Huld, T., Adams, P., & Bartzis, J.G. (2003) Source, dispersion and combustion modelling of an accidental release of hydrogen in an urban environment. *J. Hazard Mater.* 105(1):1-25.

[48] Gallego, E., Migoya, E., Martín-Valdepeñas, J.M., Crespo, A., García, J., Venetsanos, A., Papanikolaou, E., Kumar, S., Studer, E., Dagba, Y., Jordan, T., Jahn, W., Høiset, S., Makarov, D., & Piechna, J. (2007) An inter-comparison exercise of the capabilities of CFD models to predict distribution and mixing of H_2 in a closed vessel. *Int. J. Hydrogen Energy* 32:2235- 2245.

[49] Wilkening, H., & Baraldi, D. (2007) CFD modelling of accidental hydrogen release from pipelines. *Int. J. Hydrogen Energy* 32(13):2206-2215.

[50] Venetsanos, A.G., Baraldi, D., Adams, P., Heggem, P.S., & Wilkening, H. (2008) CFD modelling of hydrogen release, dispersion and combustion for automotive scenarios. *J.*

Loss Prev. Proc. Ind. 21(2)162-184.

[51] Makarov, D., Verbecke, F., Molkov, V., Roe, O., Skotenne, M., Kotchourko, A., Lelyakin, A., Yanez, J., Hansen, O., Middha, P., Ledin, S., Baraldi, D., Heitsch, M., Efimenko, A. & Gavrikov, A. (2009) An inter-comparison exercise on CFD model capabilities to predict a hydrogen explosion in a simulated vehicle refueling environment. *Int. J. Hydrogen Energy* 34(6):2800-2814.

[52] Hajji, Y., Bouteraa, M., ELCafsi, A., Belghith, A., Bournot, P., & Kallel, F. (2015) Numerical study of hydrogen release accidents in a residential garage. *Int. J. Hydrogen Energy* 40(31):9747-9759.

[53] Matsuura, K., Kanayama, H., Tsukikawa, H., & Inoue, M. (2009) Numerical simulation of leaking hydrogen dispersion behavior in a partially open space. *Int. J. Hydrogen Energy* (33)(1):240-247.

[54] Kikukawa, S. (2008) Consequence analysis and safety verification of hydrogen fueling stations using CFD simulation. *Int. J. Hydrogen Energy* 33(4):1425-1434.

[55] Liu, H., & Schreiber, W. (2008) The effect of ventilation system design on hydrogen dispersion in a sedan. *Int. J. Hydrogen Energy* 33(19):5115-5119.

[56] Salva, J.A., Tapia, E., Iranzo, A., Pino, F.J., Cabrera, J., & Rosa, F. (2012) Safety study of a hydrogen leak in a fuel cell vehicle using computational fluid dynamics. *Int. J. Hydrogen Energy* 37(6):5299-5306.

[57] Qi, D., Wang, L., & Zmeureanu, S. (2014) An analytical model of heat and mass transfer through non-adiabatic high-rise shafts during fires. *Fire Tech* 72(5): 585-594.